Acta Oceanol. Sin., 2023, Vol. 42, No. 9, P. 27–43
https://doi.org/10.1007/s13131-022-2116-z
http://www.aosocean.com
E-mail: ocean2@hyxb.org.cn

The influence of bioturbation on sandy reservoirs: the delta front sand of the lower Zhujiang Formation, Baiyun Depression, Zhujiang River Mouth Basin

Zhifeng Xing[1, 2], Wei Wu[1]*, Juncheng Liu[1], Yongan Qi[1], Wei Zheng[1]

[1] The Institute of Resources and Environment, Henan Polytechnic University, Jiaozuo 454000, China

[2] Shandong Provincial Key Laboratory of Depositional Mineralization and Sedimentary Mineral, Shandong University of Science and Technology, Qingdao 266590, China

Received 8 December 2021; accepted 26 August 2022

Abstract

Ichnofossils are well developed in clastic rock reservoirs in marine and transitional facies, which can considerably change the physical properties of the reservoir. However, this influence is not well understood, raising an important problem in the effective development of petroleum reservoirs. This paper analyzes continental shelf margin delta reservoirs through core observation, cast thin section observation and reservoir physical property test. Some important scientific insights are obtained: (1) The presence of *Cruziana* ichnofacies, including *Asterosoma*, *Ophiomorpha*, *Planolites*, *Skolithos*, *Thalassinoides*, and other ichnofossils can be used to identify in subaqueous distributary channels, subaqueous levee, frontal sheet sand, abandoned river channels, crevasse channels, main channels and channel mouth bars. Considerable differences in the types of ichnofossils and the degree of bioturbation can be observed in the different petrofacies. (2) Ichnofossils and bioturbation play a complex role in controlling reservoir properties. The reservoir physical properties have the characteristics of a decrease–increase–decrease curve with increasing bioturbation degree. This complex change is controlled by the sediment mixing and packing of bioturbation and the diagenetic environment controlled by the ichnofossils. (3) Sea-level cycle changes affect the modification of the reservoir through sediment packing. Bioturbation weakens the reservoir's physical property when sea level slowly rises and improves the reservoir's physical property when base level slowly falls.

Key words: bioturbation, reservoir physical properties, sedimentary petrofacies, shelf margin delta, Baiyun Sag

Citation: Xing Zhifeng, Wu Wei, Liu Juncheng, Qi Yongan, Zheng Wei. 2023. The influence of bioturbation on sandy reservoirs: the delta front sand of the lower Zhujiang Formation, Baiyun Depression, Zhujiang River Mouth Basin. Acta Oceanologica Sinica, 42(9): 27–43, doi: 10.1007/s13131-022-2116-z

1 Introduction

Ichnofossils are the records of organisms' activities within the environment they occupy, which include a myriad of structure types such as tracks, trails, burrows, feeding structures, and other traces produced during their lifetime (Seilacher, 2007). The types and assemblages of ichnofossils in different sedimentary environments vary greatly. Ichnofacies corresponding to different sedimentary environments can be divided into six petrofacies, including *Scoyenia*, *Skolithos*, *Cruziana*, *Glossifungites*, *Zoophycos*, and *Nereites* (Seilacher, 1967). This classification scheme has been revised and improved by later researchers (Pemberton et al., 1992; MacEachern et al., 1999). Currently, 11 ichnofacies have been identified, including three continental ichnofacies (*Scoyenia*, *Mermia*, and *Termitichnus*) and eight marine ichnofacies (*Trypanites*, *Teredolites*, *Glossifungites*, *Psilonichnus*, *Skolithos*, *Cruziana*, *Zoophycos*, and *Nereites*). Many research examples on ichnofossils and ichnofacies of deltaic environments have been provided but few studies have focused on continental shelf margin deltas (Dasgupta et al., 2016). Quantitative studies are even more scarce.

In addition to ichnofossils' significance as a facies indicator, the changes of physical properties in the reservoir caused by bioturbation are more attractive to petroleum geologists (Pemberton and Gingras, 2005; Al-Hajeri et al., 2009; Ali et al., 2010; Angulo and Buatois, 2012; Baniak et al., 2013; Knaust, 2017; Oliveira de Araújo et al., 2021). Bioturbation can be one of the primary controlling factor of reservoirs' physical properties (Al-Hajeri et al., 2009; Ali et al., 2010). Bioturbation is generally believed to have a negative effect on permeability (Al-Hajeri et al., 2009; Ali et al., 2010; Lemiski et al., 2011; Gingras et al., 2012; La Croix et al., 2013; Dey and Sen, 2017). However, several studies suggest that porosity and permeability of reservoirs can be either increased or decreased depending on the differences among filling materials by bioturbation or in sandy and carbonate reservoirs (Pemberton and Gingras, 2005; Knaust, 2017; La Croix et al., 2017; Oliveira de Araújo et al., 2021). However, the mechanism behind bioturbation effect on reservoir properties are not fully understood. Sediment particles are mixed through the organ-

Foundation item: The National Natural Science Foundation of China under contract Nos 41872112 and 42077410; the Key Research Project of Higher Education Institutions in Henan University under contract No. 20A170010; the Program for Innovative Research Team (in Science and Technology) of Henan Polytechnic University under contract No. T2022-05; the Foundation of Shandong Provincial Key Laboratory of Depositional Mineralization and Sedimentary Mineral under contract No. DMSM2018027.
*Corresponding author, E-mail: wei@hpu.edu.cn

isms' behaviors, such as burrow-dwelling, foraging, and migration, which changes the original structures, textures, and compositions and increases heterogeneity (Pemberton and Gingras, 2005). Bioturbation disrupts the primary sediment particles distribution and causes sediment mixing. High bioturbation quantities can also lead to the homogenization of bedded structure deposits and the intrusion of clay minerals, which reduces the permeability of sandy sediment (Dewhurst et al., 1998, 1999; Qi, 1998; Dornbos et al., 2000; Pemberton et al., 2004, 2008; MacEachern et al., 2007; Tonkin et al., 2010; Lemiski et al., 2011; La Croix et al., 2013; Dey and Sen, 2017; Knaust, 2017). In addition to sediment mixing, some biological activities, such as sediment cleaning can also improve the original reservoir's physical properties (Bentley and Nittrouer, 2003; Dey and Sen, 2017; Quaye et al., 2019). Some studies have found that the intrusion of coarse fragments will increase the porosity and permeability of rocks. In sand-filled burrows or interconnected burrow systems, porosity and permeability are increased in the vertical and horizontal directions as compared to cores with no bioturbation, which is of great significance for oil and gas reservoirs (Gingras et al., 2007, 2012; Pemberton and Gingras, 2005; Cunningham et al., 2009; Knaust, 2009; Tonkin et al., 2010; Baniak et al., 2015; Dey and Sen, 2017; Hsieh et al., 2017; Quaye et al., 2019; Oliveira de Araújo et al., 2021).

Continental shelf margin deltas are large, thick, wedge-shaped sedimentary bodies developed near the shelf break under the conditions of sufficient sediment supply from continental rivers and the relative decline of sea level (Porębski and Steel, 2003; Dixon et al., 2012; Lin et al., 2018a). The shelf margin delta is the link between shallow and deep-water sedimentary units, and plays an important role in the study of marine sedimentary evolution. The excellent lithologic combination of shelf margin delta and overlying transgressive sediments result in very large hydrocarbon accumulations. A large number of hydrocarbon resources were recognized in the explorations of the Gulf of Mexico, Eastern Mediterranean, East African Coast, and the South China Sea (Lin et al., 2001, 2018b; Pang et al., 2004; Petter and Steel, 2006; Wu et al., 2009, 2018, 2023; Perov and Bhattacharya, 2011; Liu et al., 2017; Zhang et al., 2017; Li et al., 2017, 2020).

Therefore, studying the ichnofossils of the sandy reservoir will enable the exploration of the physicochemical mechanisms of bioturbation affecting the reservoir's properties, expanding the understanding of the heterogeneity of sandy reservoir, and provide a theoretical basis for high precision exploration and development of petroleum reservoirs at the continental shelf margin setting, such as the lower Zhujiang Formation in Baiyun Sag in the South China Sea.

2 Geological setting

2.1 *Geological background*

The Zhujiang River Mouth Basin is located in the northern continental shelf of the South China Sea and formed during the Cenozoic extension event of the South China Sea. It can be divided into five NE-trending secondary tectonic units from north to south: Northern Uplift Belt, Northern Depression Belt, Central Uplift Belt, Southern Depression Belt, and Southern Uplift Belt. The Baiyun Sag is a third-level tectonic unit located in the Southern Depression Belt (Fig. 1) and is one of the important areas for deep-water petroleum exploration and development in the South China Sea, and is characterized by a typical continental shelf margin succession (Wu et al., 2014; Lin et al., 2018a). Zhujiang Formation is the key strata for the transformation from shallow sea to deep sea environment in Baiyun Sag, where a large number of continental shelf margin deltas, slope fans and basin floor fans are developed. Previous researchers have carried out a considerable number of studies on the sedimentary filling of the Miocene Zhujiang Formation (23.8–15.5 Ma), and they have found a large-scale shelf-margin deltas which at the lower Zhujiang Formation in the northern slope of Baiyun Sag (Shi et al., 2010; Wang et al., 2011b; Ran et al., 2015; Li et al., 2018; Yu et al., 2019). This delta has excellent reservoir-caps resulting in the massive accumulation of hydrocarbons (Zhang et al., 2017). A large number of ichnofossils have been found in the sandy reservoirs of the delta succession. Some studies have observed and described the features of some of these ichnofossils but did not explore their effects on petrophysical properties (Zheng et al., 2013; Wu et al., 2014; Liu et al., 2014).

2.2 *Tectonic evolution*

The evolution of the Baiyun Sag can be divided into three main periods: initial rifting before extension (Paleocene to middle Eocene), rifting with extension (late Eocene to early Miocene), and sedimentation after extension (middle Miocene to Present) (Xie et al, 2015). At the end of the Mesozoic, the Shenhu Movement (about 68 Ma) in the northern part of the South China Sea formed the basement of the region and the entire Zhujiang River Mouth Basin was under intense tension (Chen et al., 2003; Zhao et al., 2015; Hou et al., 2020). A series of semi-graben and graben developed in the Baiyun Sag. These structures were connected, forming a complex basin with multiple depositional centers (Zhang, 2010). During the Eocene (about 54–35.4 Ma), two stages of the Zhuqiong Movement occurred in the Zhujiang River Mouth Basin leading to period of uniform subsidence in the whole basin (Hou et al., 2020). The early/late Oligocene South China Sea Movement (about 29.3 Ma) was the strongest tectonic movement, which transformed the basin from fault depression stage to thermal subsidence depression stage (Li, 1993; Chen et al., 2012). Meanwhile, the Baiyun Movement (about 25.5–23.8 Ma) at the end of Oligocene, which occurred simultaneously with the southward migration of the spreading ridge in the South China Sea, was accompanied by strong thermal subsidence that led to the rapid transition of the northern continental shelf-slope break zone of the South China Sea from the southern to the northern side of the Baiyun Sag (Pang et al., 2007, 2008; Shao et al., 2007). The Baiyun Movement was an adjustment event of the basin structure. The water depth of the Baiyun Sag rose considerably with the northward transition of the shelf-slope break belt, while a large number of sediments from the Yanshan Fold Belt along the South China accumulated in the Baiyun Sag to form a shelf margin sedimentary system (Wu et al., 2010, 2014; Xu et al., 2011; Yi et al., 2012) (Fig. 2). Since then, the basin entered a period of relatively stability and the Baiyun Sag was covered by deep-water deposits.

2.3 *Sedimentary stratigraphy*

Several studies discussed the Neogene sequence stratigraphic framework and sedimentary environment evolution of the Baiyun Sag and its surrounding region (Fig. 2). The Zhujiang Formation on the northern slope of Baiyun Sag was divided into four third-order sequences, namely SQ23.8, SQ21, SQ17.5, and SQ16.5, based on five surfaces formed at 23.8 Ma, 21 Ma, 17.5 Ma, 16.5 Ma, and 15.5 Ma, respectively (Xie et al., 2009). SQ23.8 represent a continental rifting sequence, while SQ17.5 and SQ16.5 are deep sea sequences. SQ21 is the conversion sequence between them, which indicates that the Baiyun Sag changed from a shallow continental shelf to a semi-deep to deep-water environment (Shao et al., 2005; Pang et al., 2007; Zhu et al., 2009).

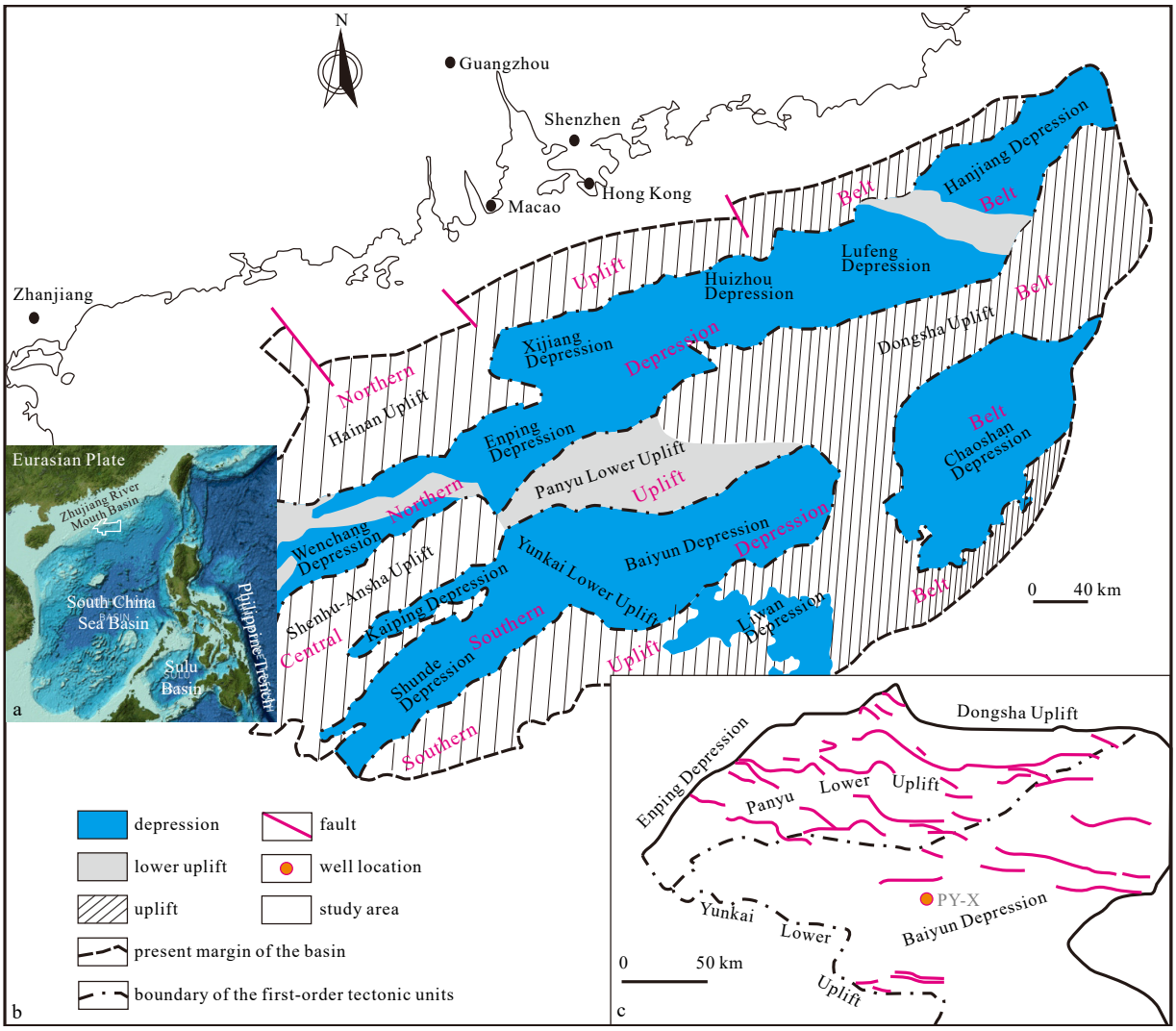

Fig. 1. Study area and location map. a. Geomorphologic features of the South China Sea; b. internal tectonic units of the Zhujiang River Mouth Basin; c. internal structure of Baiyun Depression.

Large-scale shelf-margin deltas were developed at the bottom of sequence SQ21. The sedimentary characteristics and evolution of these continental shelf margin deltas have been studied extensively (Shao et al., 2005; Pang et al., 2007; Zhu et al., 2009; Wang et al., 2011a; Xu et al., 2016; Lin et al., 2018a). At the upper continental slope break, the foreset beds, which represent the subaqueous deltaic sediments, deposited clastic rocks more than 1 000 m thick in a typical progradation structure. The development of these delta systems was controlled by factors, such as the sediment supply of the ancient Zhujiang River, the ancient submarine geomorphology, and sea level changes (Yin et al., 2011; Li et al., 2013; Wu et al., 2014). Compared with other deltas, the continental shelf margin delta front of the SQ21 has a large progradation angle and it is highly bioturbated (Wu et al., 2014). Gravity flow features have only been observed from seismic data and so far, no wells have drilled into these deep-sea deposits (Lin et al., 2018b).

2.4 *Shelf-margin deltaic reservoir related research*

Many oil and gas reservoir analyses on the shelf-margin delta of sequence SQ21 have been conducted in the study area. However, these studies have been mainly focused on the sedimentary and petrological characteristics, or on the physical properties of the reservoir. Subaqueous distributary channels, channel mouth bars, and sheet sands have been identified as the main reservoir petrofacies through the use of cores, core logging, and seismic data (Wu et al., 2010; Zhang et al., 2012; Yu et al., 2019). Some studies have analyzed the petrology and porosity through thin sections, scanning electron microscopy (SEM), mercury intrusion, and physical property analysis (Liu et al., 2017; Wang, 2016). The reservoir is characterized by significant heterogeneity, which is controlled by tectonics, sedimentary association, and diagenesis (Wan et al., 2017). Despite the numerous findings on the sedimentary tectonics and diagenesis of the reservoirs, the influence of the intense bioturbation has not received sufficient attention.

3 Research method

3.1 *Shelf-margin deltaic core observation and petrofacies identification*

During this study, the physical properties of rock samples were tested and statistically analyzed for one sample per 20 cm in the core of PY-X. A total of 135 core samples (mainly sandstone and siltstone) were taken from the lower Zhujiang Formation at depths of 3 732.05–3 758.60 m through drilling Well PY-X on the northern slope of Baiyun Sag. Based on previous studies, we sub-

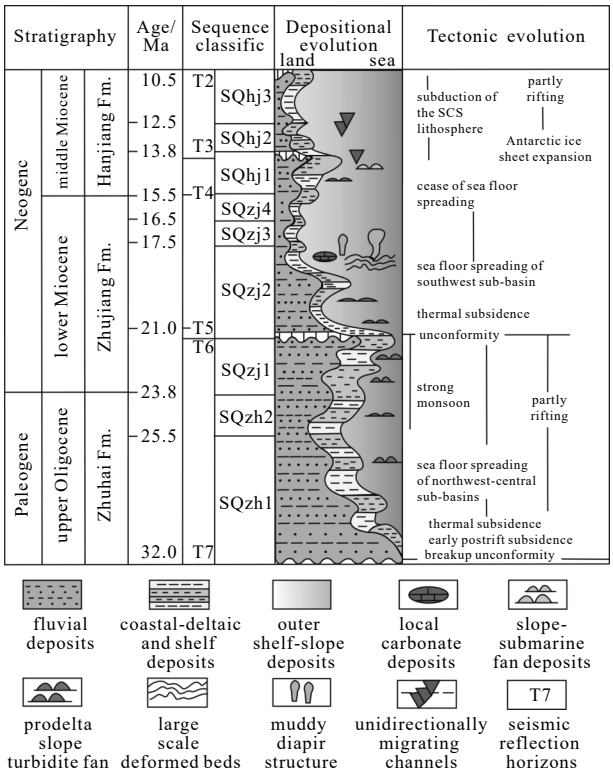

Fig. 2. Schematic summary of the depositional evolution, sequence stratigraphy framework, and main tectonic movements in the Zhujiang River Mouth Basin during the Cenozoic period (modified from Lin et al. (2018a), SQhj3: Sequence Hangjiang Fm. 3; SQzj4: Sequence Zhujiang Fm. 4; SQzh2: Sequence Zhuhai Fm. 2.

divided the six sedimentary petrofacies of the shelf-margin delta deposit using lithology, lithological associations, sedimentary textures, and sedimentary structures (especially ichnofossils). We identified and classified the trace fossils in cores by using the classic ichnofossills' profile features (Gerard and Bromley, 2008). Then, we measured the area of bioturbation in the photographs of the core with an interval of 0.1 m and the percentage of the bioturbation area in the total area was taken as an indicator of bioturbation intensity in the interval (Droser and Bottjer, 1986).

According to the characteristics of the core, rock samples were classified as non-bioturbated (0% of bioturbation intensity, NBT from here onward), weakly bioturbated (1%–20%, WBT from here onward), moderately bioturbated (21% to 60%, MBT from here onward) and pervasively bioturbated (61% to 100%, PBT from here onward) (Table 1, modified from Droser and Bottjer (1986)).

3.2 *Analysis of the physical properties of the reservoir*

The porosity and permeability of 135 rock samples in the target interval were measured by using the Core Measurement System-300, and the porosity data of the samples were compared and analyzed with their depths and bioturbation intensity. Then, 53 samples were selected and thin-sectioned. The mineral composition and pore type of these 53 samples were identified through petrographic and SEM observation. The grain size of 24 selected samples was also investigated. Finally the influence of bioturbation on the sedimentological and physical properties of the reservoir, was analyzed by comparing grain-size, pore types, and structures of samples with bioturbation intensity.

4 Results

4.1 *Petrologic characteristics*

The studied samples are mainly medium- to coarse-grained and medium- to fine-grained lithic sandstones (Fig. 3). On average they can be categorized as lithic sandstone with quartz, feldspar, and rock fragments, following Folk (1974)'s scheme of sandstone composition and genesis classification (Fig. 4). Quartz accounts for the largest proportion of all particles, about 63.8% of the total. Quartz overgrowths were observed (Fig. 3). Rock fragments are also very common (up to 35.15%) and mainly consist of metamorphic, claystone and protogenous fragments. The content of feldspar particles (mainly potassium feldspar) is very small, 1.03% on average. The overall abundance of rock fragments indicates a low maturity. In most samples, the sedimentary texture is grain-supported, displaying point-line contacts, and contact-porous cementation (Figs 3a, e). The roundness of many particles is subangular, and the sorting was poor to medium. The kaolinite-vermiculite structure (Fig. 3e) and scaly structure (Fig. 3c) are easily observed in particles. Pores are medium to well developed and are dominated by secondary solution pores. The types of pores are mainly intergranular and particle solution pores with irregular shapes. The pore connectivity is average, mainly punctuate and sheet throats.

Table 1. Bioturbated classification scheme

BI	Taylor and Goldring (1993)		Droser and Bottjer (1986)		This research scheme (modified from Droser and Bottjer (1986))	
	Bioturbated quantity/%	Classification	Bioturbated quantity/%	Classification	Bioturbated quantity/%	Classification
0	0	no-bioturbation	0	non-bioturbation	0	non-bioturbation
1	1–4	sparse bioturbation	0–10	discrete, isolated trace fossils	1–20	weakly bioturbated, massive, parallel and tabular cross bedding distinct boundaries and low discrete traces density
2	5–30	low bioturbation	10–40	burrows are generally isolated, but locally overlap		
3	31–60	moderate bioturbation	40–60	burrows overlap and are not always well defined	21–60	moderately bioturbated, massive and parallel bedding with sharp boundaries and rare discrete traces overlap
4	60–90	high bioturbation	60–100	bedding is completely disturbed, but burrows are still discrete in places and the fabric is not mixed	61–100	pervasively bioturbated, massive and inverse graded structures with indistinct to completely disturbed bedding boundaries, high trace density with common overlap to repeated overprinting
5	91–99	intense bioturbation				
6	100	complete bioturbation	100	bedding is nearly or totally homogenized		

Note: BI: bioturbation index.

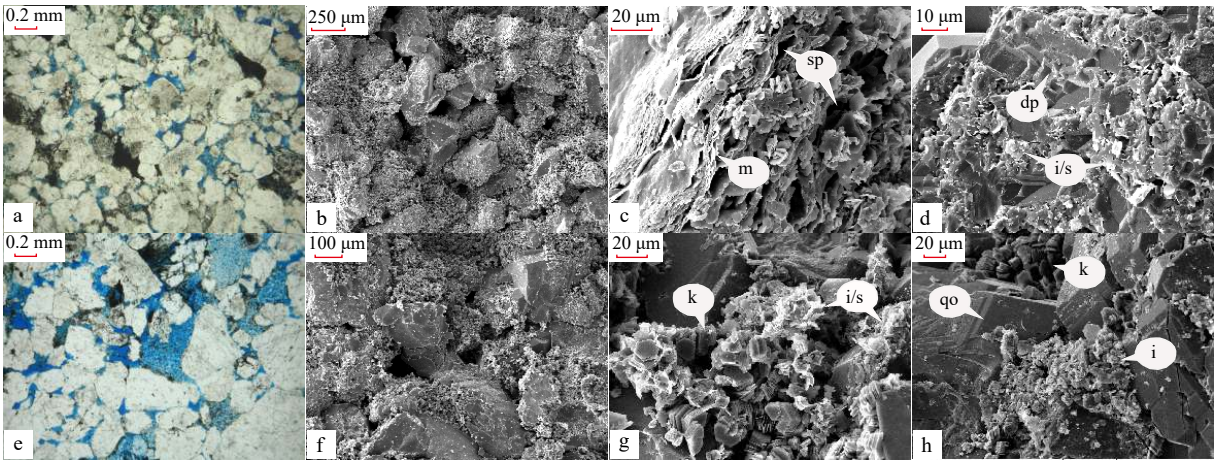

Fig. 3. Micrograph of sandstone sample. a–d. Micrograph of the sandstone sample at depth of 3 735.03 m; a. Thin section image, the sample is a medium-fine grained sandstone, where the rock is compact; b. SEM image, overall, the intergranular pores are 30–100 μm with good connectivity; c. SEM image, feldspar is altered into flaky mica (m) and solution pores (sp); d. SEM image, quartz is dissolved into dissolution pits (dp) mixed with lamellar illite/smectite (i/s) layer. e–h. Micrograph of the sandstone sample at depth of 3 742.28 m; e. Thin section image, the sample is a medium-grained sandstone, where the rock is compact; f. SEM image, overall, the intergranular pores are 20–60 μm with good connectivity; g. SEM image, intergranular lamellar illite/smectite (i/s) mixed layer and kaolinite (k); h. SEM image, intergranular flaky illite (i), kaolinite (k), quartz overgrow (qo) to Level III.

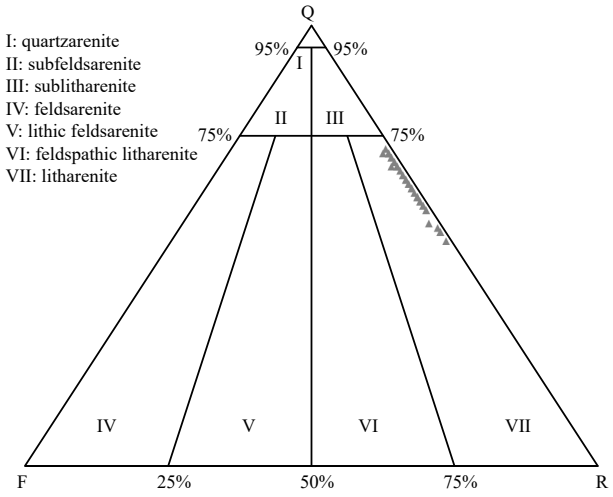

Fig. 4. Ternary plot of sandstone type of the shelf margin delta front studied sandstones.Q: quartz; F: feldspar; R: rock fragments.

4.2 *Sedimentary petrofacies*

The sedimentary assemblages were subdivided into different petrofacies according to the differences in core characteristics, such as lithology, lithological association, ichnofossil, and sedimentary structure. Six sedimentary petrofacies were identified, including subaqueous distributary channel, channel mouth bar, subaqueous levee, frontal sheet sand, abandoned channel, and crevasse channel (Fig. 5). Subaqueous distributary channel and channel mouth bar have the largest thickness (4.73 m and 20.31 m), accounting for 17.82% and 76.50% of the total thickness, respectively. The trace fossils determined are ichnogenus: *Ophiomorpha*, *Palaeophycus*, *Planolites*, *Skolithos*, and *Thalassinoides*. Traces described in open nomenclature as escape trace were also observed. This ichnofossil assemblage is typical of the *Cruziana* ichnofacies (Fig. 5).

4.2.1 *Subaqueous Distributary Channel (SDC)*

Gray medium- and coarse-grained sandstones as well as coarse-grained lithic sandstones with fine gravel characterize this petrofacies (Figs 6a–d). Sedimentary structures such as massive, parallel, normal graded bedding, tabular cross-bedding, and small cross-bedding are common in this petrofacies. Scour surfaces often developed at the bottom of the SDC facies (Fig. 6a) along with a small number of trace fossils (Figs 6a–c). The SDC sand is often consist of a number of upward-fining single sand bodies with thickness of 0.15–1.00 m. The SDC developed a variety of trace fossils, including *Bergaueria, Conichnus*, *Diplocraterion*, *Ophiomorpha*, *Planolites*, *Skolithos*, *Thalassinoides*, and escape traces (Figs 6a–c).

4.2.2 *Channel Mouth Bar (CMB)*

The CMB is composed mainly of medium- to fine-grained sandstones and some siltstones (Figs 6e–h), with inverse grading (Fig. 5). Among the CMBs, homogeneous structures are well developed and small cross beddings are partially visible. The ichnofossil structures are also well developed in CMBs. The degree of bioturbation was moderate to strong, with *Bergaueria, Diplocraterion*, *Ophiomorpha*, *Palaeophycus*, *Planolites*, *Rhizocorallium*, *Teichichnus*, and *Thalassinoides* (Figs 6e–h).

4.2.3 *Abandoned Channel and Crevasse Channel (AC and CC)*

The petrofacies of AC and CC are rare in the drilling cores (Fig. 5). The rare AC develops between two sets of SDCs, with sandy mudstone layers several centimeters thick (Fig. 6i) and contains ichnofossil structures, such as *Planolites*, *Thalassinoides*, and unidentified dwelling burrows filled with fine gravel and coarse sand (Fig. 6i). CC deposits are composed mainly of banded mudstone, thin-layered siltstone, fine-grained sandstone, coarse-grained sandstone and fine gravel interbedded with scour surfaces (Fig. 6i). The CC was covered by the AC with escape trace (Figs 5 and 6i).

4.2.4 *Frontal Sheet Sand (FSS)*

FSS occurs very infrequently in the analyzed cores (Fig. 5). The lithology of the FSS was composed mainly of gray medium- to fine-grained sandstone, with parallel, swash cross, and rare inverse graded bedding (Fig. 5). The FSS developed a small num-

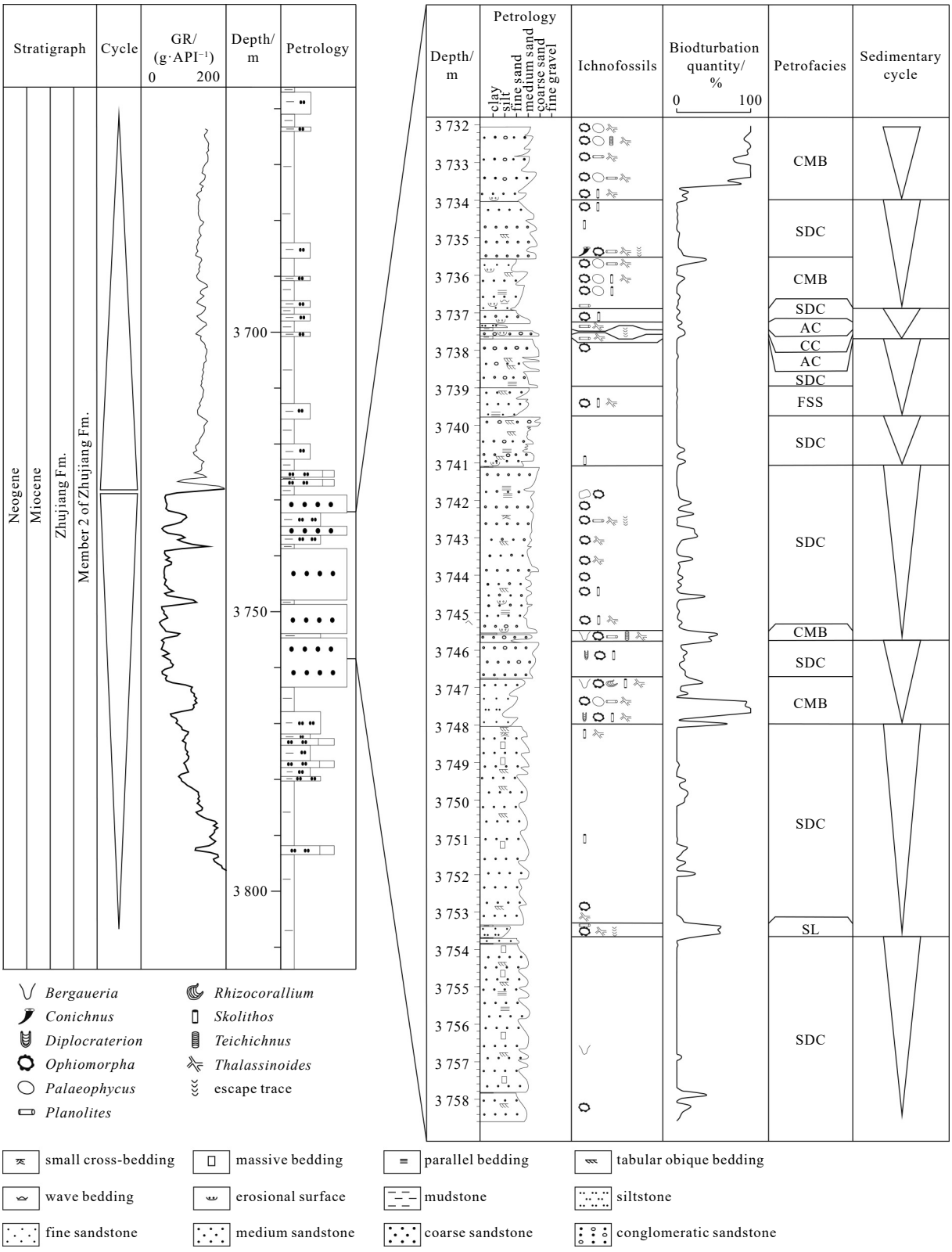

Fig. 5. Sedimentation and bioturbation profile of Well PY-X. CMB: Channel Mouth Bar; SDC: Subaqueous Distributary Channel; CC: Crevasse Channel; AC: Abandoned Channel; FSS: Frontal Sheet Sand; SL: Subaqueous Levee; GR: gamma ray log.

ber of ichnofossils, such as *Ophiomorpha*, *Skolithos*, and *Thalassinoides* (Figs 6j, k).

4.2.5 *Subaqueous Levee (SL)*

SL facies occurs very infrequently in the studied cores and generally has a very thin thickness of about 30 cm (Fig. 5). The lithology of the SL consists of sandstone, siltstone, and muddy siltstone with massive structure. The parallel beddings between the muddy and silty lamina layers interbedded were partially visible (Fig. 6l). The degree of bioturbation was moderate to strong, with

Ophiomorpha, *Planolites*, *Thalassinoides*, and escape traces (Fig. 6l).

4.3 *Bioturbation intensity in sedimentary cycles*

Water depth, sedimentation rate, salinity, turbidity, oxygenation, matrix consistency, hydrodynamic energy, and event deposition, control the bioturbation, activity range, and behaviors (Frey et al., 1990; Taylor et al., 2003; Gingras et al., 2011). The shelf-margin delta front is characterized by high sedimentation rate, high slope, overall shallow water, and strong hydrodynamic energy (Porębski and Steel, 2003). The constant change in such a sedimentary environment formed nine regressive sedimentary cycles, which combined with a higher level transgressive cycle by identification according to petrological characteristics and sedimentary petrofacies (Fig. 5). Each sedimentary cycle is composed of one or more petrofacies, and the trace fossil associations in different cycles are quite different. We found that various bioturbation intensity within the cores ranges between 0% and 100% (Fig. 5). In SDC petrofacies, biotrubated levels ranges from NBT to WBT, and few small parts of MBT, with bioturbation intensity of 0%–35%. On the contrary, the bioturbated level of the CMB petrofacies was mostly PBT and few MBT, with bioturbation intensity range of 50%–100%. The bioturbated level of SL petrofacies was mostly MBT with bioturbation intensity range of 45%–55%. The bioturbation level of AC, CC, and FSS petrofacies are all WBT with a bioturbation intensity less than 10%. Combining the composition of the petrofacies in the nine secondary cycles, we established the petrofacies model of shelf-margin delta front with the distribution of ichnofossils (Fig. 7). The model contains two medium-severe bioturbation layers that correspond to the CMB and SL. These sedimentary grains are fine sandstone and medium sandstone, indicating that the environments were moderately hydrodynamic (Li et al., 2008). Fewer ichnofossils and weak bioturbation were found in the lower part of the SDC, FSS, AC, and CC. The SDC with medium-coarse sandstone was formed in high-energy hydrodynamics environments (Li et al., 2008, 2016). The FSS, AC, and CC, in which bioturbation is relatively scarce, formed in low-energy settings accordingly, and the bioturbation distributes horizontally along with the bedding.

4.4 *Reservoir physical characteristics*

A comparative analysis of porosity and permeability in core physical properties shows that porosity and permeability have similar trends with depth and exhibit a logarithmic relationship

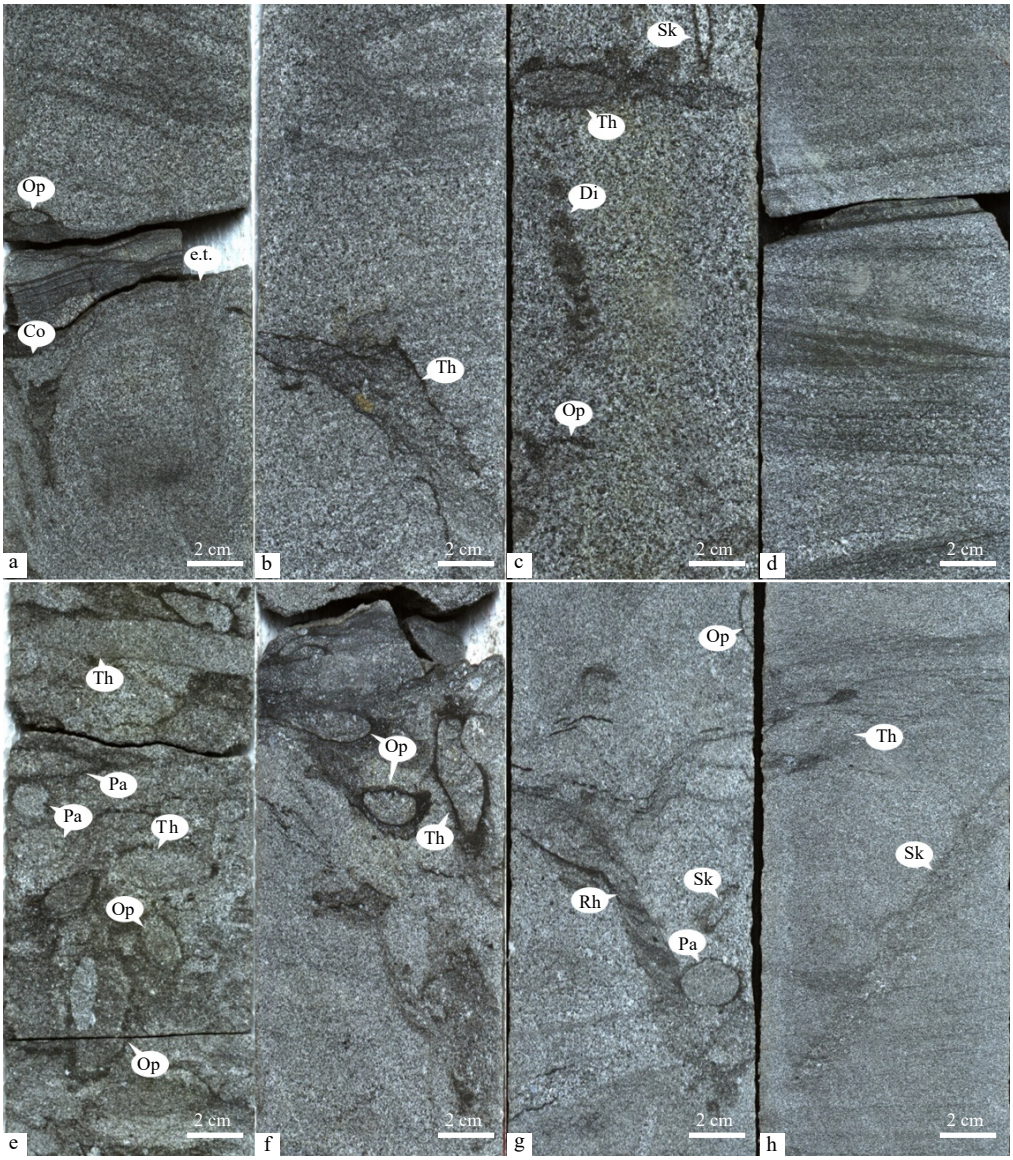

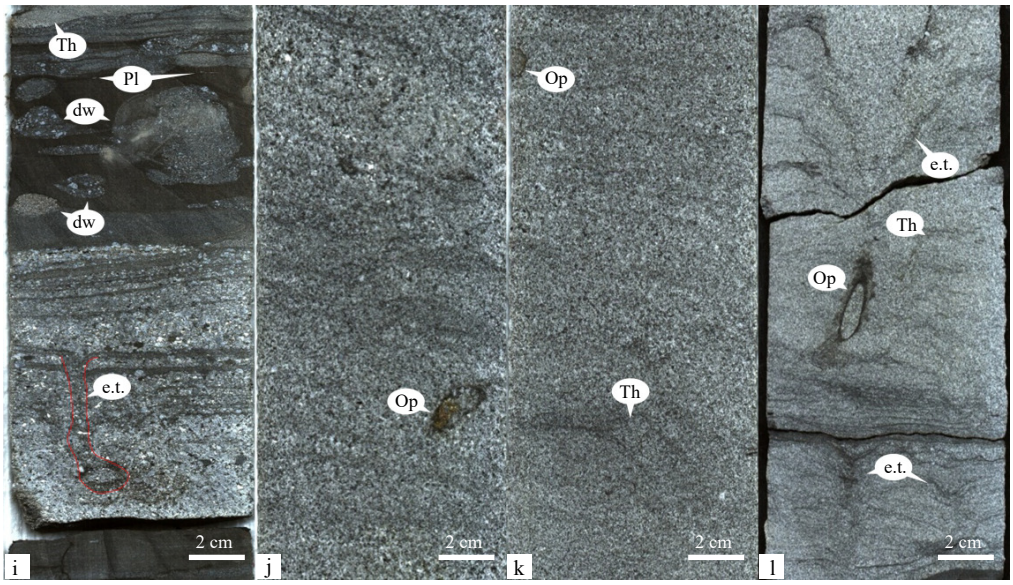

Fig. 6. Sedimentary characteristics of petrofacies. a–d. Sedimentary characteristics of subaqueous distributary channel. a. 3 735.33–3 735.50 m, fine-, medium-, to coarse-grained sandstone with tabular cross-bedding in the upper part. *Conichnus* (Co), *Ophiomorpha* (Op), and escape trace (e.t.) are contained near the scour surface. b. 3 742.83–3 743.00 m, medium- to coarse-grained massive sandstone with *Thalassinoides* (Th). c. 3 746.00–3 746.16 m, medium- to coarse-grained sandstone with massive bedding with *Diplocraterion* (Di), *Ophiomorpha* (Op), *Skolithos* (Sk), and *Thalassinoides* (Th). d. 3 750.31–3 750.45 m, fine-, medium- to coarse-grained sandstone, with parallel bedding in the upper part and small cross-bedding in the lower part. e–h. Sedimentary characteristics of the channel mouth bar. e. 3 732.86–3 733.04 m, fine- to medium-grained sandstone with fine gravel with *Ophiomorpha* (Op), *Palaeophycus* (Pa), and*Thalassinoides* (Th). f. 3 745.54–3 745.68 m, fine-grained sandstone at the bottom, muddy stripe thereon, and scour surface at the top. g. 3 746.81–3 746.93 m, fine- to medium-grained sandstone with *Ophiomorpha* (Op), *Palaeophycus* (Pa), *Rhizocorallium* (Rh), and *Skolithos* (Sk). h. 3 746.99–3 747.20 m, fine-grained sandstone with *Skolithos* (Sk) and *Thalassinoides* (Th) and inverse graded bedding. i. Sedimentary characteristics of the abandoned channel and crevasse channel, 3 737.39–3 737.63 m; the bottom is gray coarse-grained sandstone with fine gravel of the crevasse channel, with discontinuous muddy lamination and escape trace (e.t.). Above it is the development of dark gray mudstone with *Planolites* (Pl) and unidentified dwelling burrows (dw) filled with medium- to coarse-grained sand. The top is a thin layer of silty sandstone in the abandoned channel with ripple cross lamination and *Thalassinoides* (Th) filled with medium-grained sand. j. Sedimentary characteristics of the frontal sheet sand, 3 739.30–3 739.45 m, fine- to medium-grained sandstone with inverse graded bedding and *Ophiomorpha* (Op). k. Frontal sheet sand, 3 739.56–3 739.68 m, contained *Ophiomorpha* (Op) and *Thalassinoides* (Th). l. Sedimentary characteristics of the subaqueous levee, 3 753.51–3 753.67 m, the lower is siltstone and fine-grained sandstone with muddy laminae and *Ophiomorpha* (Op), *Thalassinoides* (Th), escape trace (e.t.), the upper is fine- to medium-grained sandstone.

with prominent correlation (Figs 8a, b). It can be seen from all sample statistics (Fig. 8a) that bioturbation deteriorates the porosity and permeability in the physical properties of the reservoir. This result is very obvious in the severe bioturbation interval (Fig. 8c). Correspondingly, in the weak bioturbation and medium bioturbation interval, there is no obvious pattern (Fig. 8c).

The bioturbation and physical properties in sandstones composed of different particle sizes were analyzed and the relationships between the bioturbation quantity and porosity are as follows (Fig. 9a). In fine-grained sandstone, porosity goes through a process of decrease–increase–decrease with the increase of bioturbation, which corresponds to weak (Fig. 9b), medium, and severe bioturbation. In medium-grained sandstone, the variation of porosity is similar to that in fine sandstone despite the absence of medium bioturbation samples (Fig. 9c). In coarse-grained sandstone, only non-bioturbation and weak bioturbation were found and the overall effect on porosity was not obvious (Fig. 9d).

Particle sorting can change remarkably with sediment mixing and sediment packing produced through biological activities (Dey and Sen, 2017). The 53 rock samples observed through the cast thin sections were mostly medium- to coarse-grained sand and a small amount of fine-grained sand in Well PY-X. In fine-grained sandstone, the particle size-frequency distributions in NBT, WBT (Fig. 10a), and MBT (Fig. 10b) all display an unimodal distribution with a main peak at about Φ =2.125. PBT samples, display a bimodal distribution with two peaks at Φ =1.875 and Φ =3.125 (Fig. 10c), respectively. PBT brought abundant amounts of very fine-grained particles, which greatly changed particle size composition. In the medium- to fine-grained sandstone, the particle size frequency distribution of NBT, WBT (Fig. 10c), and MBT samples (Fig. 10e) also present an unimodal distribution with a peak at Φ =1.875. In PBT samples (Fig. 10f), the frequency distribution of the particle size is bimodal, with peaks at Φ =1.875 and Φ =3.125. These findings show that a PBT bioturbation brought a large amount of fine-grained particles and matrix, which greatly changed the particle size composition ratio of medium and fine-grained sandstone. No severe bioturbation features were found in coarse-grained sandstones. The particle size and frequency distributions of NBT, WBT (Fig. 10g), and MBT (Fig. 10h) are all bimodal, with peak values of Φ =0.625 and Φ =1.875, respectively.

Then we further analyzed the relationship between bioturbation intensity and reservoir physical characteristics.

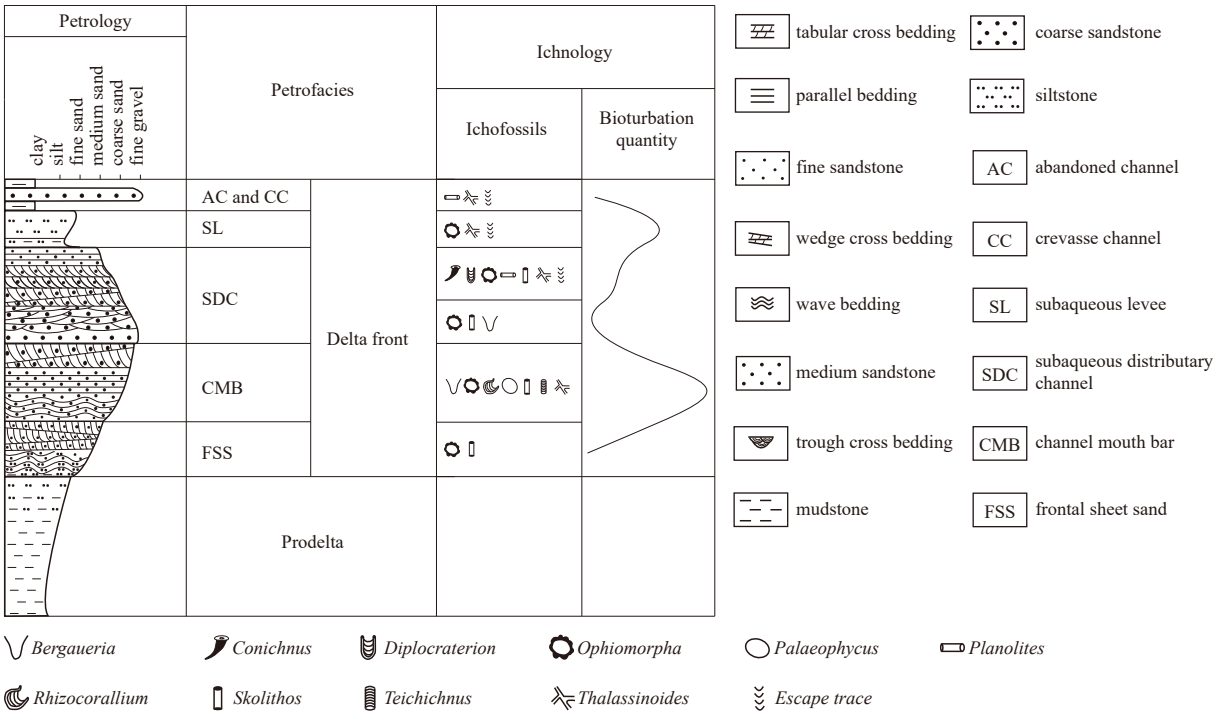

Fig. 7. Model of shelf margin delta front subfacies.

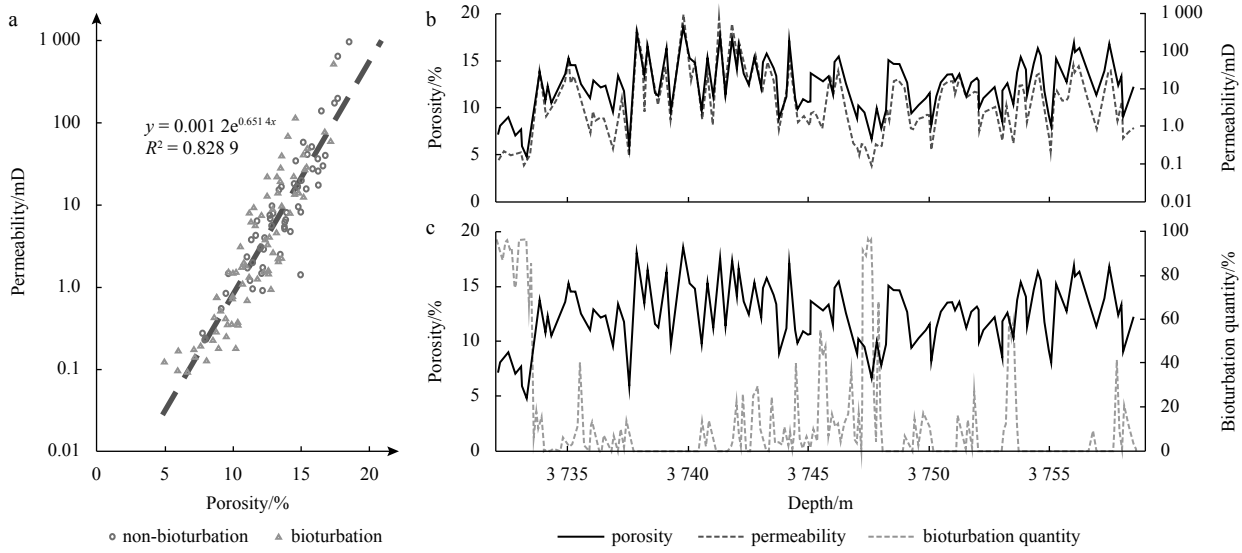

Fig. 8. Diagram of core porosity, permeability, and bioturbation quantity in Well PY-X; a. Porosity and permeability crossplot; b. curves of porosity and permeability with depth; c. curves of porosity and bioturbation quantity with depth.

4.4.1 *Non-bioturbated (NBT) to weakly bioturbated (WBT)*

In NBT or WBT samples (Fig. 11), the particles display average sorting, and most of the them are in point-line contact. The pores are generally well developed with good connectivity. Although quartz overgrowths are obvious, the residual primary pores retain a certain amount of space, that play an important role in total porosity. The secondary pores are more developed and the space of moldic porosity is larger. In general, secondary pores, including secondary intergranular and intragranular pores, occupy more space than primary pores (Fig. 11).

4.4.2 *Moderately bioturbated (MBT)*

In samples with MBT (Fig. 12), particles have poor to moderate sorting and are in point-line contact. The pores are well developed with good connectivity. Primary pores are still preserved in small quantities but secondary pores including mold, secondary intergranular, and secondary intragranular pores (Figs 12a, b), dominate in porosity. In some fine-grained sandstone samples, particles display concavo-convex contact. Microcracks are occasionally observed and the size of the particles on the two sides of the fracture is completely different (Fig. 12c). On the whole, primary pores are severely damaged, but secondary pores are very well developed.

4.4.3 *Pervasively bioturbated (PBT)*

In PBT samples (Fig. 13), particles are poorly sorted and

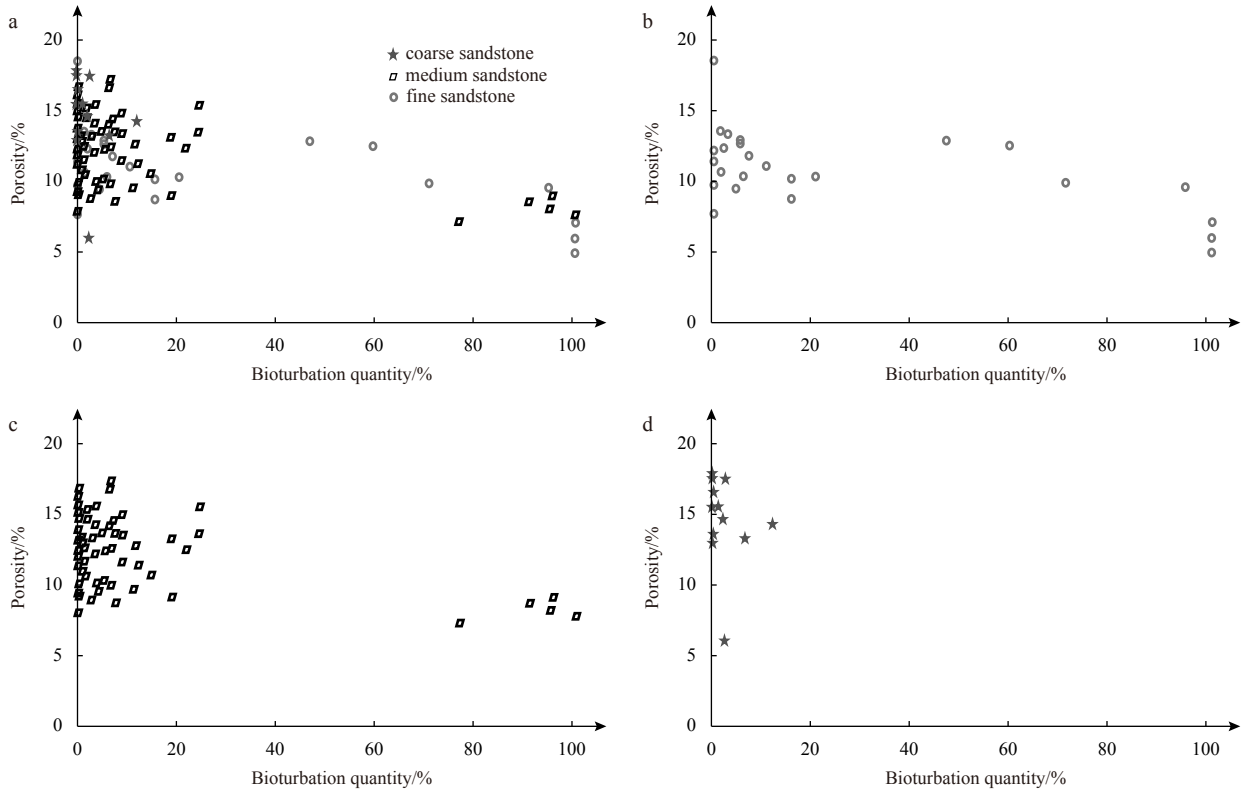

Fig. 9. Relationship between bioturbation quantity and porosity. a. Relationship between bioturbation quantity and porosity in Well PY-X; b. relationship between bioturbation quantity and porosity of fine-grained sandstone samples; c. relationship between bioturbation quantity and porosity of medium-grained sandstone samples; d. relationship between bioturbation quantity and porosity of coarse-grained sandstone samples.

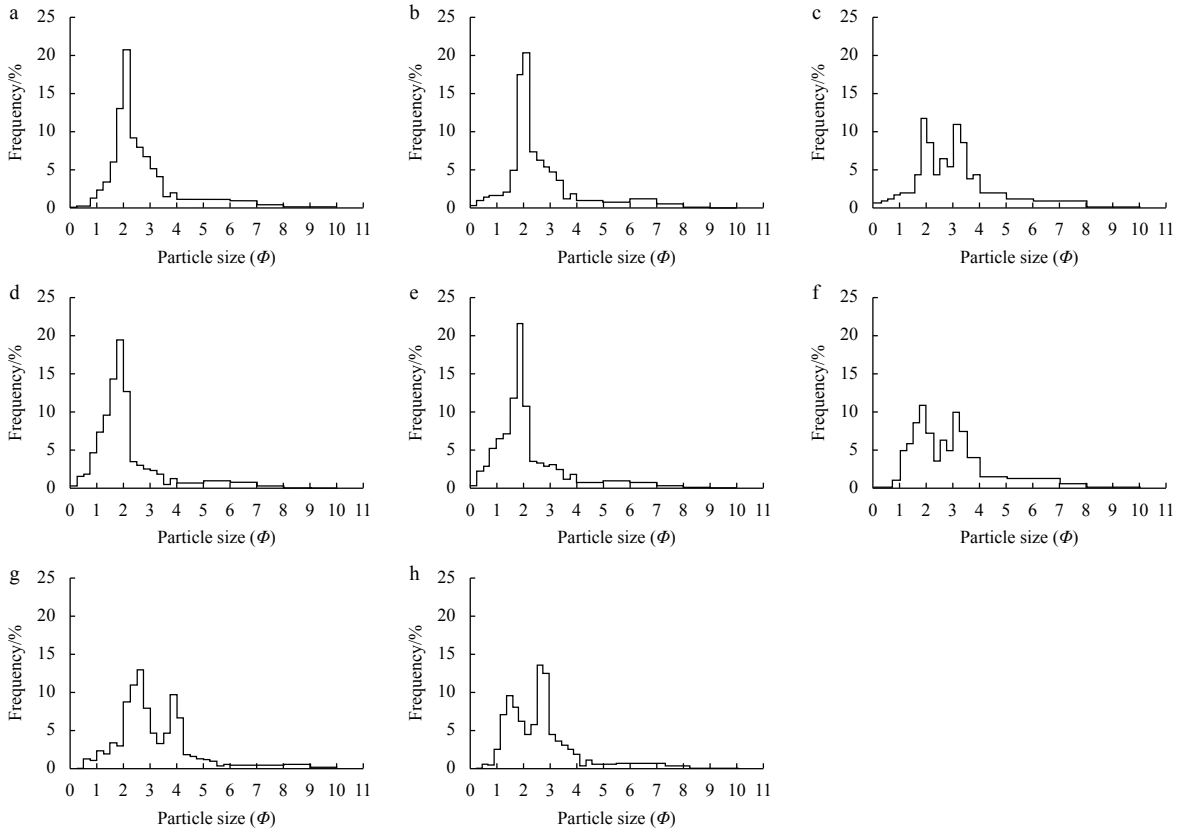

Fig. 10. Particle size distribution of samples in Well PY-X. Non-bioturbated (NBT) or weakly bioturbated (WBT) samples (a, d, g); moderately bioturbated (MBT) samples (b, e, h); prevasively bioturbated (PBT) samples (c, f).

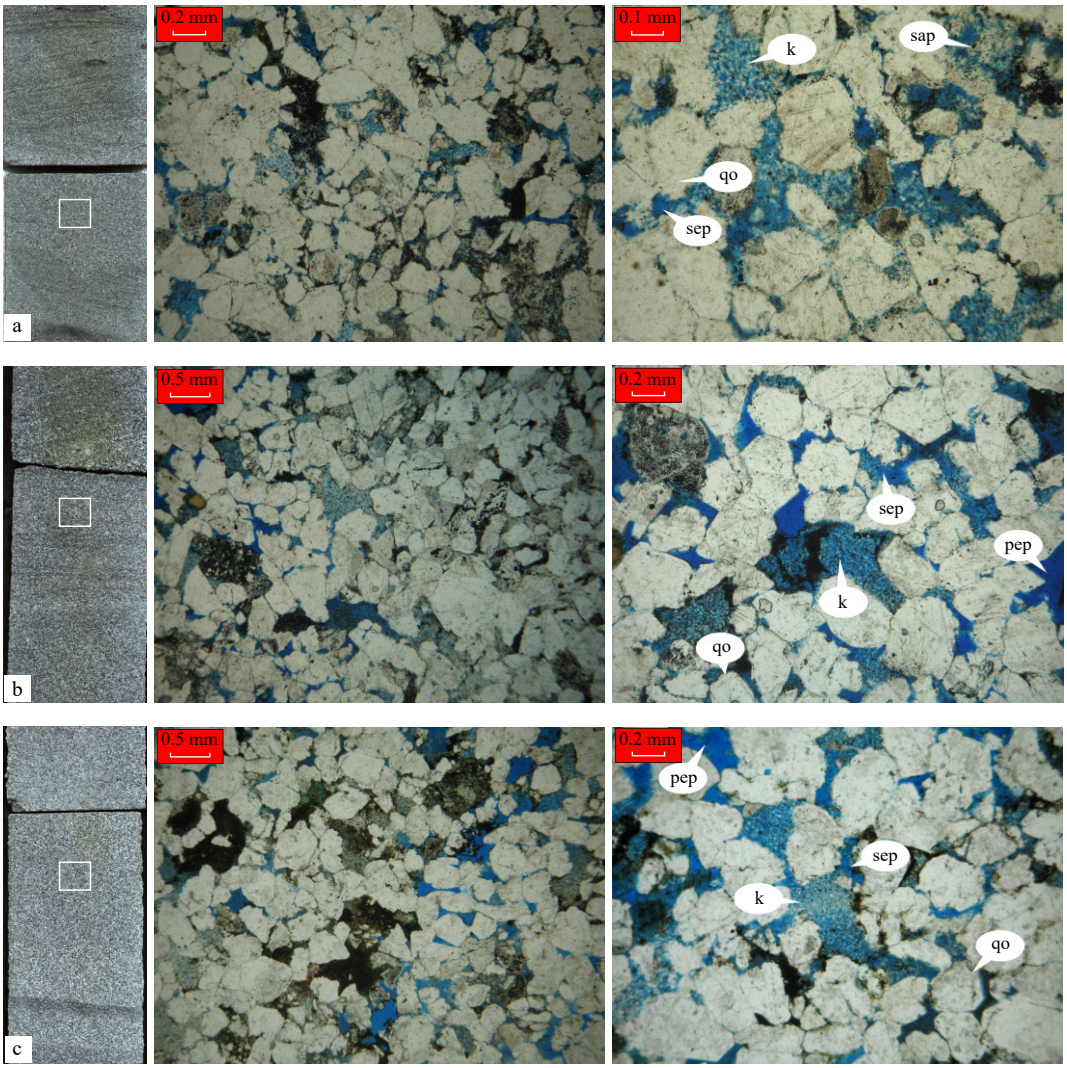

Fig. 11. Thin-sectioned characteristics of sandstone samples with NBT or WBT. a. 3 736.03 m, medium- to fine-grained sandstone, medium sorting degree, point-line contact, contact-porous cementation type. Particles are mainly fine-grained sands, and some are medium- and very fine-grained sands. The pores are moderately developed and are distributed uniformly. The secondary is the main type, including secondary inter-granular pores (sep), secondary intra-granular pores (sap), and mold pores. The pore shape is irregular and the size is generally between 0.10 mm and 0.25 mm. The shape of the primary intergranular pores is mainly triangular and irregular, and the size is generally between 0.05 mm and 0.15 mm. Kaolinite (k) and quartz overgrow (qo) can be observed. b. 3 750.78 m, medium- to fine-grained sandstone, medium sorting degree, point-line contact, contact-porous cementation type. Particles are mainly medium-grained sand, some are coarse-grained sand and a small amount of fine-grained sand. The pores are mainly secondary pores with the inhomogeneous distribution. Their types are mainly secondary intergranular (sep) and granular dissolving pores with irregular shapes that have a general size of 0.15 mm and 0.40 mm. Primary intergranular pores (pep) are scarce. Kaolinite (k) and quartz overgrow (qo) can be observed. c. 3 756.28 m, medium- to coarse-grained sandstone, medium to a poor sorting degree, point-line contact, contact-porous cementation type. Particles are mainly medium- and coarse-grained sand. The pores are generally well developed. The pores are mainly secondary pores, including mold pores and secondary intergranular pores (sep). The pore shape is mainly irregular, and the size is generally between 0.15–0.60 mm. The shape of the primary intergranular pores (pep) is mainly triangular and irregular, and the size is generally 0.10–0.20 mm. Kaolinite (k) and quartz overgrow (qo) can be observed.

either display point-line contacts or concavo-convex contacts. The pores have poor or no connectivity. Secondary intergranular and intragranular dissolved pores are the main pore type, and the primary intergranular pores are rarely developed or even underdeveloped. These findings may be due to the sediment mixing of bioturbation, which brought in a large amount of finer-grained sediments, making the rocks compact and the intergranular pores smaller, leading to a decrease in primary porosity.

5 Discussion

5.1 *Modification of sediments through bioturbation*

5.1.1 *Sediment mixing and sediment packing*

The bimodal distributions of coarse-grained sandstones represent the difference in particle transporting mode, such as coarse-grained rolling and medium-grained jumping transport methods in the channel (Figs 10c, f). With the increase of bi-

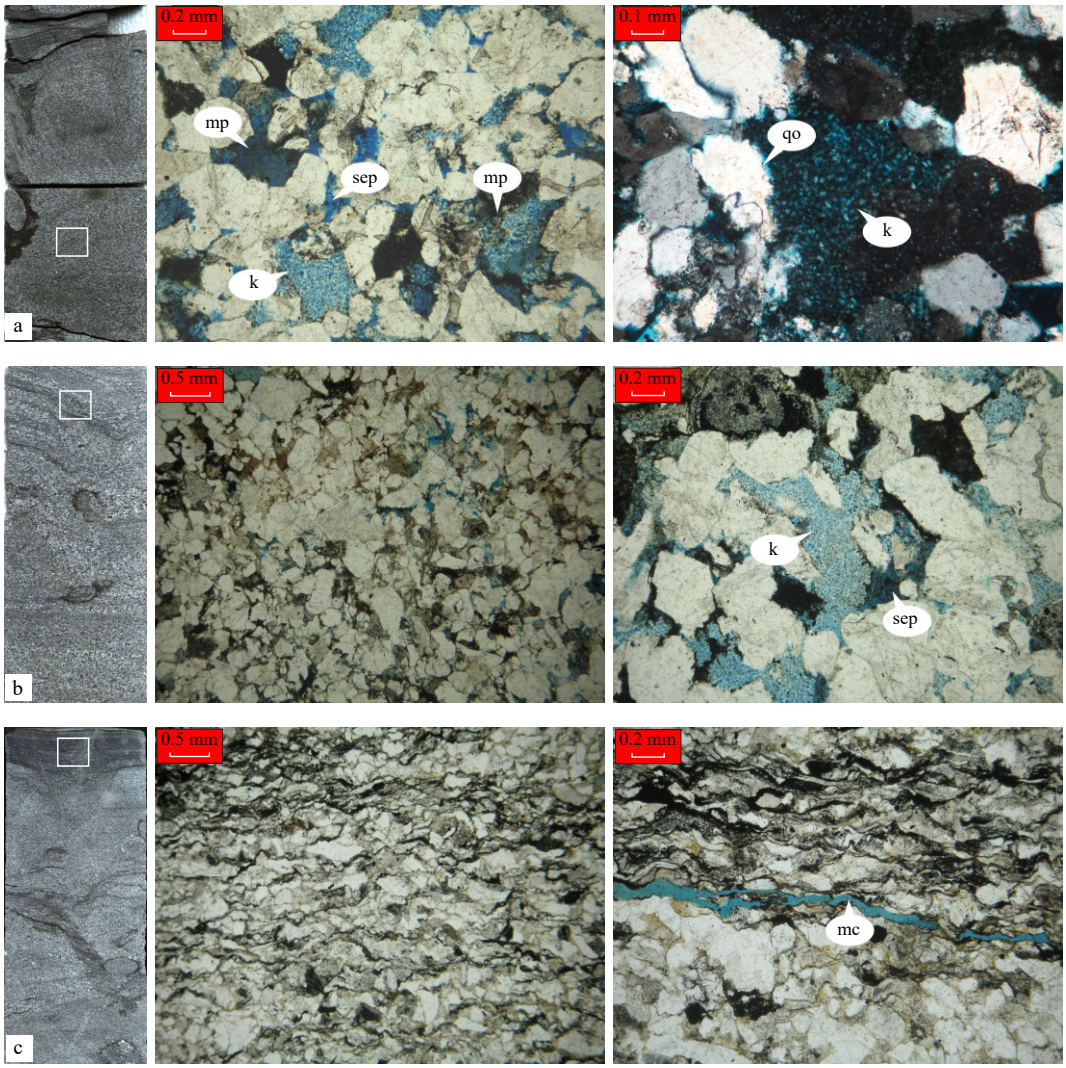

Fig. 12. Thin-sectioned characteristics of sandstone samples with MBT. a. 3 735.53 m, medium- to coarse-grained sandstone, poor to medium sorting degree, point-line contact, and contact-pore cementation type. The amount of medium-grained sand particles is slightly higher than that of coarse-grained sand particles and small amounts of fine-grained sand particles also occur. The pores are moderately developed and uniformly distributed. The secondary pores, including mold pores (mp) and secondary intergranular pores (sep), represents the most common kind of pore. The shape of the secondary intergranular pores is irregular and their size is generally between 0.10–0.25 mm. Kaolinite (k) and quartz overgrow (qo) can be observed. b. 3 743.78 m, medium- to coarse-grained sandstone, poor to medium sorting degree, point-line contact, porous cementation type. The amount of medium-grained sands particles is slightly higher than that of coarse-grained sand particles, and a small amount of fine-grained sand praticles can also be observed. The pores, mainly secondary pores, are poorly developed and uniformly distributed, such as secondary intergranular pores (sep). The shape is irregular, and the size is generally between 0.10–0.30 mm. The primary pores are mainly intergranular pores with poor connectivity. Kaolinite (k) can be observed. c. 3 746.80 m, medium- to fine-grained sandstone, poor to medium sorting degree, concavo-convex contact, and porous cementation type. The amount of fine-grained sand particles is slightly higher than that of medium-grained sand particles, and a small amount of coarse-grained sand particles can also be observed. Microcracks (mc) can occasionally be observed with widths of 0.03–0.05 mm.

oturbation, the grain size distribution changes from unimodal (Figs 10a, b) to become coaser (Figs 10d, e) and then to bimodal (Figs 10g, h) in fine- and medium-grained to fine-grained sandstone. In PBT samples of fine- and medium-grained to fine-grained sandstone, the distinct bimodal distribution was caused by abundant foreign particles with different particle sizes, which were carried by the trace maker. In bioturbated samples, sediment mixing and sediment packing changed the original particles composition and physical properties of sedimentary rocks. The former implies a change in the previous arrangement of particles within the sediment, while the latter focuses on the trace maker filling the burrow with foreign particles.

5.1.2 *Sediment packing and sea level change*

Because of the many possible combinations of bioturbation intensity and sedimentary mixing due to trace-maker activity, whether the sediment becomes coarser or finer due to bioturbation is complex. Improvement of sandy reservoir physical properties occurs where burrow fills are more coarse-grained than the host rock (Pemberton and Gingras, 2005; Lemiski et al., 2011; Friesen et al., 2017). Horizontal biological activities and internal sediment mixing do not cause drastic changes in particle size,

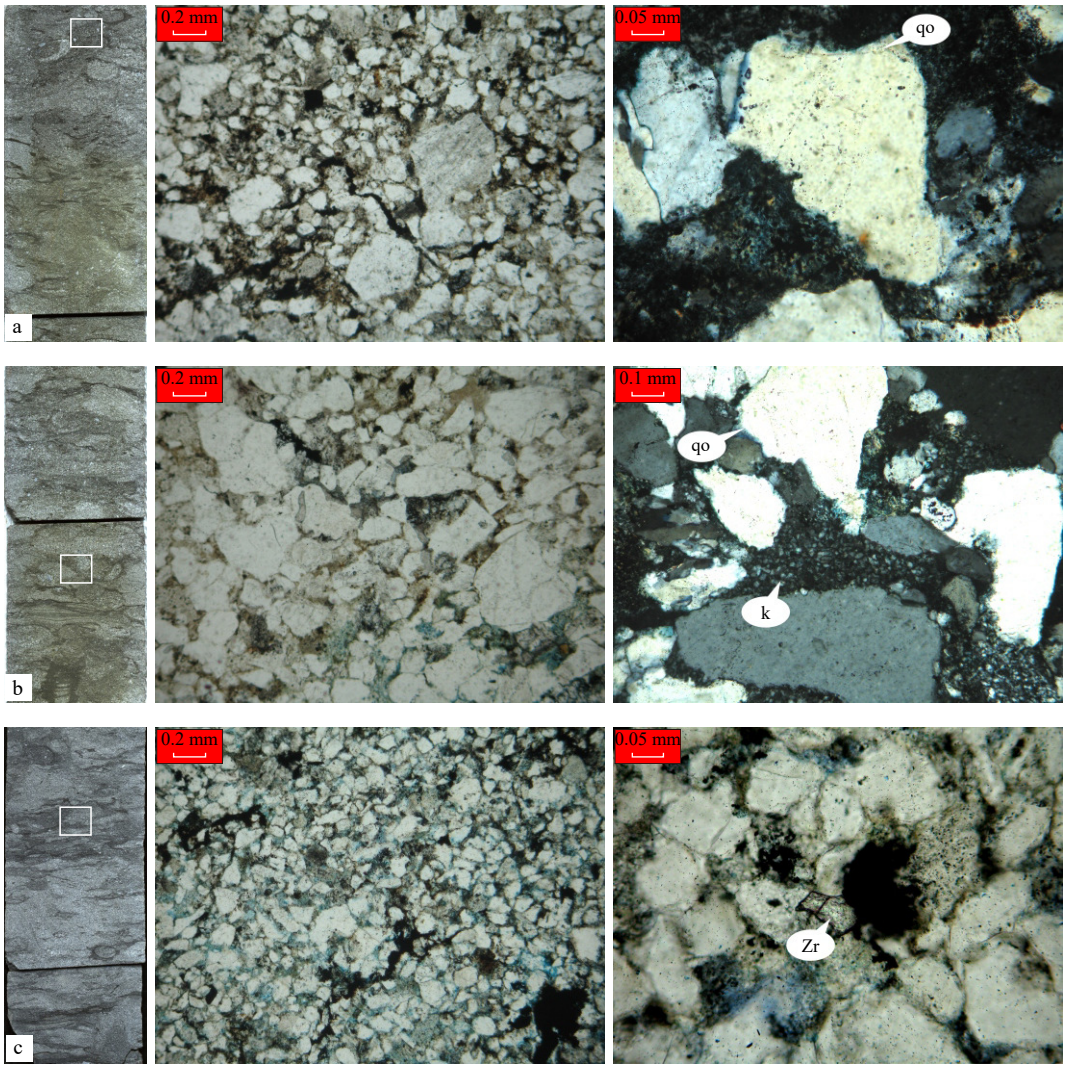

Fig. 13. Thin-sectioned characteristics of sand samples with severe bioturbation from various ichnogenus. a. 3 732.07 m, medium- to fine-grained sandstone, poor to medium sorting degree, point-line contact, and porous cementation type. Fragment particles are mainly silty and fine-grained sands, with fewer medium-grained particles. The pores are poorly developed, distributed in homogeneously, and are mainly secondary dissolved pores with poor connectivity. Quartz overgrow (qo) can be observed. b. 3 732.53 m, medium- to fine-grained sandstone, poor sorting degree, point-line contact, and porous cementation type. Particles are contained in all grades, including fine-, medium-, and coarse-grained. Pores are poorly developed and granular and intergranular dissolved pores can occasionally be observed with poor connectivity. Kaolinite (k) and quartz overgrow (qo) can be observed. c. 3 747.66 m, fine-grained sandstone, medium to a good sorting degree, point-line contact, porous cementation type. Particles are mainly fine-grained with a small amount of medium-grained sands. The pores are poorly developed. Zircon (Zr) can occasionally be observed.

while vertical biological bioturbation can greatly change the particle composition in host sediments. Changes in the sedimentary environment, such as regression-transgression, hydrodynamic conditions, and sediment supply can result in large vertical variations of grain-size (Catuneanu et al., 2011). In our study, the relative sea-level changes control the sediment particle size change under the influence of bioturbation. When the relative sea level falls, overlying sediment particles are relatively coarse, and the vertical burrows bring coarser sediments into host sediments, thereby increasing the mixing sediment particle size (Figs 14a, b, g). On the contrary, when the relative sea level rises, the overlying sediment particles are finer and vertical burrows bring fine-grained sediments into the host rock, resulting in a decrease in the mixing sediment particle size (Figs 14c, f). These changes are all slow rises and falls of the relative sea level, but a too abrupt environmental change may also cause a change in the behavior of trace makers, such as a shift from vertical to horizontal activity (Figs 14d, e), which would do little to alter the particle size distribution (Gingras et al., 2012).

5.2 *Effects of bioturbation on reservior quality*

The effects of bioturbation on reservoir physical properties are not unidirectional and simple. Some strata show that pervasive ichnofossils penetrating the rock matrix, result in remarkably improved porosity and permeability (Gingras et al., 2012; Oliveira de Araújo et al., 2021), although numerous studies have shown that bioturbation has a negative effect on porosity and permeability (Al-Hajeri et al., 2009; Ali et al., 2010; Lemiski et al., 2011; Gingras et al., 2012; La Croix et al., 2013; Dey and Sen, 2017). The physical properties we investigated belong to the main reservoir petrofacies, such as SDC and CMB, which represent different deposition during a relative sea level falling (Fig. 9a).

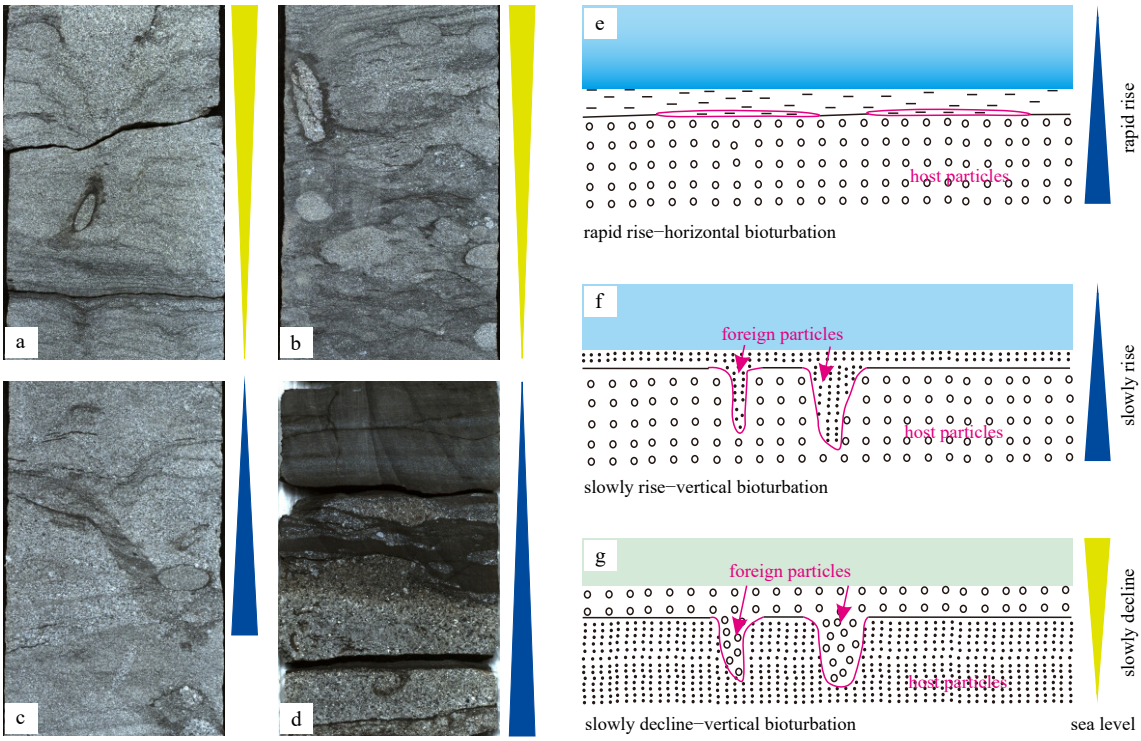

Fig. 14. Base level change and bioturbation effect on reservoir properties. Base level decline (a, b); base level rise (c, d); the model of the bioturbation effect on reservoir properties (e, f, g).

Understanding the mechanism of bioturbation, the reservoir physical properties focused mainly on sediment mixing, sediment packing, and sediment cleaning of bioturbation (Pemberton and Gingras, 2005; Ali et al., 2010; Tonkin et al., 2010; Gingras et al., 2012; Qi et al., 2012; Baniak et al., 2013; Dey and Sen, 2017; Quaye et al., 2019; Oliveira de Araújo et al., 2021), which were more likely to affect the primary physical properties. Sediment mixing varies greatly with different biological activities, including vertical and horizontal bioturbation (Fig. 9). Horizontal bioturbation tends to weaken particle sorting and breaks sand laminae, leading to the redistribution of fine clay particles and a decline in the overall porosity and permeability of sediments (Gingras et al., 2012; Dey and Sen, 2017). The effects of vertical bioturbation on reservoir physical properties are very complicated and depend on the vertical variation of sediment particle size becoming coarser or finer due to bioturbation (Gingras et al., 2012; Dey and Sen, 2017). When the overlying sediment particles are coarser than the host reservoir, the coarser foreign particles improve the physical properties of the host reservoir. In contrast, finer foreign particles resulted in the worsening of the final physical properties (Baniak et al., 2015; Dey and Sen, 2017). The differences between foreign and host particles are determined by slow changes in the relative sea level and hydrodynamic intensity (Buatois and Mángano, 2011; Rodríguez et al., 2018). Therefore, the sediment mixing of horizontal bioturbation causes the primary physical properties of the reservoir to worsen, while the influence of sediment mixing of vertical bioturbation on the transformation of the primary physical property is related to environmental change. In the rock record, the preserved patterns of permeability and porosity are strongly influenced by the characteristics of the burrow filling sediment, the property of burrow backfilling, compaction, and cementation (Dirk and Richard, 2012). Concerning secondary dissolution pores, sediment mixing may change the primary porosity and permeability of the reservoir, thus influencing diagenetic processes and the generation of secondary porosity (Baniak et al., 2013; Knaust, 2017).

6 Conclusions

The sandstones of the shelf-margin delta of the lower Zhujiang Formation are mainly moderately immature medium-fine to coarse-grained lithic sandstones. The core of Well PY-X can be divided into six sedimentary petrofacies: subaqueous distributary channels, channel mouth bars, subaqueous levee, frontal sheet sands, abandoned river channels, and crevasse channels. The trace fossil diversity and abundance are low in the middle part of the subaqueous distributary channel, frontal sheet channel sand, and abandoned river channels, but high at the top and bottom of the channels and other petrofacies.

The studied deposits represent a large transgressive cycle composed of nine secondary regressive cycles. A complete delta front cycle is interpreted. Many types of trace fossils can be found in the upper part of the channel mouth bar and subaqueous distributary channel. The bioturbation in channel mouth bar and the subaqueous levee has a greater intensity and abundance.

The rock samples were divided into three types: weak, moderate, and severe bioturbation. As the degree of bioturbation increases, the porosity and permeability in the reservoir physical properties have change features of decrease–increase–decrease, which is a comprehensive manifestation of bioturbation activity, such as sediment mixing, sediment packing, and sediment cleaning.

The study show that sea-level changes control the influence of bioturbation on petrophysical properties. When the sea level slow rises, bioturbation reduces the physical properties of the reservoir and it improves them when the base level slowly decreases.

Acknowledgements

We thank the editor and two anonymous experts for their constructive suggestions.

References

Al-Hajeri M M, Al Saeed M, Derks J, et al. 2009. Basin and petroleum system modeling. Oilfield Review, 21(2): 14–29

Ali S A, Clark W J, Moore W R, et al. 2010. Diagenesis and reservoir quality. Oilfield Review, 22(2): 14–27

Angulo S, Buatois L A. 2012. Integrating depositional models, ichnology, and sequence stratigraphy in reservoir characterization: The middle member of the Devonian-Carboniferous Bakken Formation of subsurface southeastern Saskatchewan revisited. AAPG Bulletin, 96(6): 1017–1043, doi: 10.1306/11021111045

Baniak G M, Gingras M K, Burns B A, et al. 2015. Petrophysical characterization of bioturbated sandstone reservoir facies in the Upper Jurassic Ula Formation, Norwegian North Sea, Europe. Journal of Sedimentary Research, 85(1): 62–81, doi: 10.2110/jsr.2015.05

Baniak G M, Gingras M K, Pemberton S G. 2013. Reservoir characterization of burrow-associated dolomites in the Upper Devonian Wabamun Group, Pine Creek gas field, central Alberta, Canada. Marine and Petroleum Geology, 48: 275–292, doi: 10.1016/j.marpetgeo.2013.08.020

Bentley S J, Nittrouer C A. 2003. Emplacement, modification, and preservation of event strata on a flood-dominated continental shelf: Eel shelf, Northern California. Continental Shelf Research, 23(16): 1465–1493, doi: 10.1016/j.csr.2003.08.005

Buatois L A, Mángano M G. 2011. Ichnology: Organism-substrate Interactions in Space and Time. Cambridge: Cambridge University Press, 358

Catuneanu O, Galloway W E, Kendall C G St C, et al. 2011. Sequence stratigraphy: Methodology and Nomenclature. Newsletters on Stratigraphy, 44(3): 173–245, doi: 10.1127/0078-0421/2011/0011

Chen Changmin, Shi Hesheng, Xu Shice, et al. 2003. The Condition of Hydrocarbon Accumulation of Tertiary Petroleum System in Pearl River Mouth Basin (East) (in Chinese). Beijing: Science Press

Chen Weitao, Du Jiayuan, Long Gengsheng, et al. 2012. Analysis on controlling factors of marine sequence stratigraphy evolution in Pearl River Mouth Basin. Acta Sedimentologica Sinica (in Chinese), 30(1): 73–83

Cunningham K J, Sukop M C, Huang Haibo, et al. 2009. Prominence of ichnologically influenced macroporosity in the karst Biscayne aquifer: Stratiform "super-K" zones. Geological Society of America Bulletin, 121(1–2): 164–180

Dasgupta S, Buatois L A, Mángano M G. 2016. Living on the edge: evaluating the impact of stress factors on animal-sediment interactions in subenvironments of a shelf-margin delta, the Mayaro Formation, Trinidad. Journal of Sedimentary Research, 86(9): 1034–1066, doi: 10.2110/jsr.2016.47

Dewhurst D N, Aplin A C, Sarda J P, et al. 1998. Compaction-driven evolution of porosity and permeability in natural mudstones: An experimental study. Journal of Geophysical Research: Solid Earth, 103(B1): 651–661, doi: 10.1029/97JB02540

Dewhurst D N, Aplin A C, Sarda J P. 1999. Influence of clay fraction on pore-scale properties and hydraulic conductivity of experimentally compacted mudstones. Journal of Geophysical Research: Solid Earth, 104(B12): 29261–29274, doi: 10.1029/1999JB900276

Dey J, Sen S. 2017. Impact of bioturbation on reservoir quality and production-a review. Journal of the Geological Society of India, 89(4): 460–470, doi: 10.1007/s12594-017-0629-4

Dirk K, Richard G B. 2012. Trace Fossils as Indicators of Sedimentary Environments. Amsterdam: Elsevier, 64: 105–129

Dixon J F, Steel R J, Olariu C. 2012. Shelf-edge delta regime as a predictor of deep-water deposition. Journal of Sedimentary Research, 82(9): 681–687, doi: 10.2110/jsr.2012.59

Dornbos S Q, Phelps W, Bottjer D J, et al. 2000. Effects of bioturbation on reservoir sandstone porosity and permeability: Studies of outcrop samples from the Upper Cretaceous, Book Cliffs, Utah (abs.). AAPG Annual Meeting Program 9, A40

Droser M L, Bottjer D J. 1986. A semiquantitative field classification of ichnofabric. Journal of Sedimentary Research, 56(4): 558–559, doi: 10.1306/212F89C2-2B24-11D7-8648000102C1865D

Frey R W, Pemberton S G, Saunders T D A. 1990. Ichnofacies and bathymetry: a passive relationship. Journal of Paleontology, 64(1): 155–158, doi: 10.1017/S0022336000042372

Friesen O J, Dashtgard S E, Miller J, et al. 2017. Permeability heterogeneity in bioturbated sediments and implications for waterflooding of tight-oil reservoirs, Cardium Formation, Pembina Field, Alberta, Canada. Marine and Petroleum Geology, 82: 371–387, doi: 10.1016/j.marpetgeo.2017.01.019

Gerard J, Bromley R. 2008. Ichnofabrics in Clastic Sediments: Applications to Sedimentological Core Studies, a Practical Guide. Madrid: R. F. Gerard

Gingras M K, Baniak G, Gordon J, et al. 2012. Porosity and permeability in bioturbated sediments. In: Developments in Sedimentology. Amsterdam: Elsevier, 64: 837–868

Gingras M K, Bann K L, MacEachern J A, et al. 2007. A conceptual framework for the application of trace fossils. In: MacEachern J A, Bann K L, Gingras M K, et al. , eds. SEPM Short Course Notes. Tulsa: Society of Economic Paleontologists and Mineralogists, 1–25

Gingras M K, MacEachern J A, Dashtgard S E. 2011. Process ichnology and the elucidation of physico-chemical stress. Sedimentary Geology, 237(3–4): 115–134, doi: 10.1016/j.sedgeo.2011.02.006

Hou Yuanli, Shao Lei, Qiao Peijun, et al. 2020. Provenance of the Eocene-Miocene sediments in the Baiyun Sag, Pearl River Mouth Basin. Marine Geology & Quaternary Geology (in Chinese), 40(2): 19–28

Hsieh A I, Allen D M, MacEachern J A. 2017. Upscaling permeability for reservoir-scale modeling in bioturbated, heterogeneous tight siliciclastic reservoirs: Lower Cretaceous Viking Formation, Provost Field, Alberta, Canada. Marine and Petroleum Geology, 88: 1032–1046, doi: 10.1016/j.marpetgeo.2017.09.023

Knaust D. 2009. Ichnology as a tool in carbonate reservoir characterization: a case study from the Permian-Triassic Khuff Formation in the Middle East. GeoArabia, 14(3): 17–38, doi: 10.2113/geoarabia140317

Knaust D. 2017. Atlas of Trace Fossils in Well Core: Appearance, Taxonomy and Interpretation. Gewerbestrasse: Springer, 13–24

La Croix A D, Gingras M K, Pemberton S G, et al. 2013. Biogenically enhanced reservoir properties in the Medicine Hat gas field, Alberta, Canada. Marine and Petroleum Geology, 43: 464–477, doi: 10.1016/j.marpetgeo.2012.12.002

La Croix A D, Maceachern J A, Ayranci K, et al. 2017. An ichnological-assemblage approach to reservoir heterogeneity assessment in bioturbated strata: Insights from the Lower Cretaceous Viking Formation, Alberta, Canada. Marine and Petroleum Geology, 86: 636–654, doi: 10.1016/j.marpetgeo.2017.06.024

Lemiski R T, Hovikoski D J, Pemberton D S G, et al. 2011. Sedimentological ichnological and reservoir characteristics of the low-permeability, gas-charged Alderson Member (Hatton gas field, southwest Saskatchewan): Implications for resource development. Bulletin of Canadian Petroleum Geology, 59(1): 27–53, doi: 10.2113/gscpgbull.59.1.27

Li Pinglu. 1993. Cenozoic tectonic movement in the Pearl River Mouth Basin. China Offshore Oil and Gas (Geology) (in Chinese), 7(6): 11–17

Li Dongyi, Chen Jian, Wang Aijun, et al. 2008. Recent progress in sediment transport research in Minjiang Estuary. Marine Science Bulletin (in Chinese), 27(2): 111–116

Li Xiaoping, Liu Baojun, Ding Lin, et al. 2016. Depositional elements definition of marine delta and significance to sand body correlation in petroleum exploration: From hydrodynamic analysis on modern Pearl River Delta. Acta Sedimentologica Sinica (in Chinese), 34(3): 555–562

Li Wenjing, Wang Yingmin, He Min, et al. 2018. Types and controlling factors of shelf margin delta of Middle Miocene in Pearl River Mouth Basin. Lithologic Reservoirs (in Chinese), 30(2): 58–66

Li Quan, Wu Wei, Liang Jianshe, et al. 2020. Deep-water channels in the lower Congo basin: Evolution of the geomorphology and depositional environment during the Miocene. Marine and

Petroleum Geology, 115: 104260, doi: 10.1016/j.marpetgeo.2020.104260
Li Quan, Wu Wei, Yu Shui, et al. 2017. The application of three-dimensional seismic spectral decomposition and semblance attribute to characterizing the deepwater channel depositional elements in the Taranaki Basin of New Zealand. Acta Oceanologica Sinica, 36(9): 79–86, doi: 10.1007/s13131-017-1113-0
Li Yun, Zheng Rongcai, Yang Baoquan, et al. 2013. Provenance and its geological implications of Miocene Zhujiang Formation in Baiyun Sag, Pearl River Mouth Basin. Geological Review (in Chinese), 59(1): 41–51
Lin Changsong, He Min, Steel R J, et al. 2018a. Changes in inner- to outer-shelf delta architecture, Oligocene to Quaternary Pearl River shelf-margin prism, northern South China Sea. Marine Geology, 404: 187–204, doi: 10.1016/j.margeo.2018.07.009
Lin Changsong, Jiang Jing, Shi Hesheng, et al. 2018b. Sequence architecture and depositional evolution of the northern continental slope of the South China Sea: Responses to tectonic processes and changes in sea level. Basin Research, 30: 568–595, doi: 10.1111/bre.12238
Lin Changsong, Liu Jingyan, Cai Shixiang, et al. 2001. Depositional architecture and developing settings of large-scale incised valley and submarine gravity flow systems in the Yinggehai and Qiongdongnan basins, South China Sea. Chinese Science Bulletin, 46(8): 690–693, doi: 10.1007/BF03182838
Liu Entao, Wang Hua, Uysal I T, et al. 2017. Paleogene igneous intrusion and its effect on thermal maturity of organic-rich mudstones in the Beibuwan Basin, South China Sea. Marine and Petroleum Geology, 86: 733–750, doi: 10.1016/j.marpetgeo.2017.06.026
Liu Weiqing, Wu Wei, Qin Chenggang, et al. 2014. Analysis on the sandstone reservoir by SEM: A case study of the delta front sand body of Zhujiang Formation, Baiyun Sag. Journal of Chinese Electron Microscopy Society (in Chinese), 33(2): 117–122
MacEachern J A, Bann K L, Pemberton S G, et al. 2007. The ichnofacies paradigm: high-resolution paleoenvironmental interpretation of the rock record. In: SEPM Short Course Notes. Tulsa: Society of Economic Paleontologists and Mineralogists, 52: 27–64
MacEachern J A, Zaitlin B A, Pemberton S G. 1999. A sharp-based sandstone of the Viking Formation, Joffre Field, Alberta, Canada; criteria for recognition of transgressively incised shoreface complexes. Journal of Sedimentary Research, 69(4): 876–892, doi: 10.2110/jsr.69.876
Oliveira de Araújo O M, Aguilera O, Coletti G, et al. 2021. X-ray microcomputed tomography of burrow-related porosity and permeability in shallow-marine equatorial carbonates: A case study from the Miocene Pirabas Formation, Brazil. Marine and Petroleum Geology, 127: 104966, doi: 10.1016/j.marpetgeo.2021.104966
Pang Xiong, Chen Changmin, Peng Dajun, et al. 2008. Basic geology of Baiyun deep-water area in the northern South China Sea. China Offshore Oil and Gas (in Chinese), 20(4): 215–222
Pang Xiong, Chen Changmin, Shao Lei, et al. 2007. Baiyun Movement, a great tectonic event on the Oligocene-Miocene boundary in the Northern South China Sea and its implications. Geological Review (in Chinese), 53(2): 145–151
Pang Xiong, Yang Shaokun, Zhu Ming, et al. 2004. Deep-water fan systems and petroleum resources on the northern slope of the South China Sea. Acta Geologica Sinica (English Edition), 78(3): 626–631
Pemberton S G, Gingras M K. 2005. Classification and characterizations of biogenically enhanced permeability. AAPG Bulletin, 89(11): 1493–1517, doi: 10.1306/07050504121
Pemberton S G, MacEachern J A, Frey R W. 1992. Trace fossil facies models: environmental and allostratigraphic significance. In: Walker R G, James N P, eds. Facies Models: Response to Sea Level Change. Stittsville Ontario: Geological Association of Canada, 47–72
Pemberton S G, MacEachern J A, Gingras M K, et al. 2008. Biogenic chaos: Cryptobioturbation and the work of sedimentologically friendly organisms. Palaeogeography, Palaeoclimatology, Palaeoecology, 270(3–4): 273–279
Pemberton S G, MacEachern J A, Saunders T. 2004. Stratigraphic applications of substrate-specific ichnofacies: Delineating discontinuities in the rock record. Geological Society of London, 228(1): 29–62
Perov G, Bhattacharya J P. 2011. Pleistocene shelf-margin delta: Intradeltaic deformation and sediment bypass, northern Gulf of Mexico. AAPG Bulletin, 95(9): 1617–1641, doi: 10.1306/01271109141
Petter A L, Steel R J. 2006. Hyperpycnal flow variability and slope organization on an Eocene shelf margin, Central Basin, Spitsbergen. AAPG Bulletin, 90(10): 1451–1472, doi: 10.1306/04240605144
Porębski S J, Steel R J. 2003. Shelf-margin deltas: Their stratigraphic significance and relation to deepwater sands. Earth-Science Reviews, 62(3–4): 283–326, doi: 10.1016/S0012-8252(02)00161-7
Qi Yong'an. 1998. Relations between bioturbation structures and petrophysical properties of Donghe sandstone reservoirs in central Tarim. Oil and Gas Geology (in Chinese), 19(4): 318–320
Qi Yong'an, Wang Min, Zheng Wei, et al. 2012. Calcite cements in burrows and their influence on reservoir property of the Donghe Sandstone, Tarim Basin, China. Journal of Earth Science, 23(2): 129–141, doi: 10.1007/s12583-012-0238-5
Quaye J A, Jiang Zaixing, Zhou Xuewen. 2019. Bioturbation influence on reservoir rock quality: A case study of Well Bian-5 from the second member Paleocene Funing Formation in the Jinhu Sag, Subei Basin, China. Journal of Petroleum Science and Engineering, 172: 1165–1173, doi: 10.1016/j.petrol.2018.09.026
Ran Huaijiang, Lin Changsong, Zhu Xiaomin, et al. 2015. Deposit features and control factors of low stands in deep water areas of Neocene in the northern South China Sea. Special Oil & Gas Reservoirs (in Chinese), 22(3): 46–50
Rodríguez W, Buatois L A, Mángano M G, et al. 2018. Sedimentology, ichnology, and sequence stratigraphy of the Miocene Oficina Formation, Junín and Boyacá areas, Orinoco Oil Belt, Eastern Venezuela Basin. Marine and Petroleum Geology, 92: 213–233, doi: 10.1016/j.marpetgeo.2018.01.037
Seilacher A. 1967. Bathymetry of trace fossils. Marine Geology, 5(5–6): 413–428, doi: 10.1016/0025-3227(67)90051-5
Seilacher A. 2007. Trace Fossil Analysis. Berlin, Heidelberg: Springer, 1–226
Shao Lei, Lei Yongchang, Pang Xiong, et al. 2005. Tectonic evolution and its controlling for sedimentary environment in Pearl River Mouth Basin. Journal of Tongji University: Natural Science (in Chinese), 33(9): 1177–1181
Shao Lei, Pang Xiong, Chen Changmin, et al. 2007. Terminal Oligocene sedimentary environments and abrupt provenance change event in the northern South China Sea. Geology in China (in Chinese), 34(6): 1022–1031
Shi Hesheng, Liu Baojun, Yan Chengzhi, et al. 2010. Hydrocarbon accumulation conditions and exploration potential in Baiyun-Liwan deepwater area, Pearl River Month Basin. China Offshore Oil and Gas (in Chinese), 22(6): 369–374
Taylor A M, Goldring R. 1993. Description and analysis of bioturbation and ichnofabric. Journal of the Geological Society, 150(1): 141–148, doi: 10.1144/gsjgs.150.1.0141
Taylor A, Goldring R, Gowland S. 2003. Analysis and application of ichnofabrics. Earth-Science Reviews, 60(3–4): 227–259, doi: 10.1016/S0012-8252(02)00105-8
Tonkin N S, McIlroy D, Meyer R, et al. 2010. Bioturbation influence on reservoir quality: A case study from the Cretaceous Ben Nevis Formation, Jeanne d'Arc Basin, offshore Newfoundland, Canada. AAPG bulletin, 94(7): 1059–1078, doi: 10.1306/12090909064
Wan Qionghua, Liu Weixin, Luo Wei, et al. 2017. Reservoir quality differences and major factors controlling low-permeability reservoirs of Oilfield A in the Lufeng Sag, Pearl River Mouth Basin. Oil & Gas Geology (in Chinese), 38(3): 551–560
Wang Daifu. 2016. Petrological characteristics of Zhujiang Formation and its influence on reservoir physical properties in Baiyun Sag. Ground Water (in Chinese), 38(1): 193–194, 208

Wang Yongfeng, Wang Yingmin, Li Dong, et al. 2011a. Characteristics of the slope break zones and their controls on the depositional systems in the Pearl River Mouth Basin. Sedimentary Geology and Tethyan Geology (in Chinese), 31(3): 1–6

Wang Yongfeng, Wang Yingmin, Li Dong, et al. 2011b. Characteristics of reservoirs in the Pearl River Mouth Basin. Oil Geophysical Prospecting (in Chinese), 46(6): 952–960

Wu Shiguo, Han Qinghua, Ma Yubo, et al. 2009. Petroleum system in deepwater basins of the northern South China Sea. Journal of Earth Science, 20(1): 124–135, doi: 10.1007/s12583-009-0014-3

Wu Wei, Li Quan, Yu Jing, et al. 2018. The Central Canyon depositional patterns and filling process in east of Lingshui Depression, Qiongdongnan Basin, northern South China Sea. Geological Journal, 53(6): 3064–3081, doi: 10.1002/gj.3143

Wu Wei, Liu Weiqing, Lin Changsong, et al. 2014. Sedimentary evolution of the Lower Zhujiang Group continental shelf edge in the north slope of Baiyun Sag, Pearl River Mouth Basin. Acta Geologica Sinica (in Chinese), 88(9): 1719–1727

Wu Wei, Wang Guangxu, Liu Weiqing. 2023. Quantitative morphometric analysis of a deep-water channel in the Taranaki Basin, New Zealand. Acta Oceanologica Sinica, 42(5): 42–56, doi: 10.1007/s13131-022-2024-2

Wu Jingfu, Xu Qiang, Zhu Yanhe. 2010. Generation and evolution of the shelf-edge delta in Oligocene and Miocene of Baiyun Sag in the South China Sea. Earth Science-Journal of China University of Geosciences (in Chinese), 35(4): 681–690, doi: 10.3799/dqkx.2010.083

Xie Lihua, Lin Changsong, Dong Wei, et al. 2009. High-resolution sequence stratigraphy of Zhujiang Formation and Zhuhai Formation in Panyu low uplift of the Zhujiang River Mouth Basin. Geology in China (in Chinese), 36(2): 366–377

Xie Xinong, Ren Jianye, Wang Zhenfeng, et al. 2015. Difference of tectonic evolution of continental marginal basins of South China Sea and relationship with SCS spreading. Earth Science Frontiers (in Chinese), 22(1): 77–87

Xu Yong, Chen Guojun, Ma Ming, et al. 2016. Sedimentary characteristic and evolution of Late Oligocene to Early Miocene in Baiyun depression, Pearl River Mouth Basin. Coal Geology & Exploration (in Chinese), 44(3): 1–9

Xu Qiang, Wang Yingmin, Lü Ming, et al. 2011. Identification of the shelf margin delta in sequence stratigraphic frameworks and its significance: A case study of the Baiyun Sag, South China Sea. Oil & Gas Geology (in Chinese), 32(5): 733–742

Yi Xuefei, Zhang Changmin, Li Shaohua, et al. 2012. Identification marks and depositional model of the shelf-margin delta from NSQ2 of the Pearl River Mouth Basin, China. Journal of Chengdu University of Technology: Science & Technology Edition (in Chinese), 39(3): 257–261

Yin Jun, Zhang Shangfeng, Du Jiayuan, et al. 2011. Sequence stratigraphy of the Zhujiang Formation in the Panyu area of the Pearl River Mouth Basin. Special Oil & Gas Reservoirs (in Chinese), 18(3): 56–59

Yu Ye, Zhang Changmin, Zhu Rui, et al. 2019. Characteristics and main controlling factors of the shelf-edge delta of the lower member of Zhujiang Formation in the northern Baiyun Depression. Marine Geology & Quaternary Geology (in Chinese), 39(3): 28–39

Zhang Gongcheng. 2010. Tectonic evolution of deepwater area of northern continental margin in South China Sea. Acta Petrolei Sinica (in Chinese), 31(4): 528–533

Zhang Gongcheng, Wu Tang, Xie Xiaojun, et al. 2017. Petroleum geological characteristics of two basin belts in southern continental margin in South China Sea. Petroleum Exploration and Development (in Chinese), 44(6): 849–859

Zhang Changmin, Zhang Shangfeng, Zhu Rui, et al. 2012. Recognition criteria for sand injectites in the Zhujiangkou Basin and their significance in petroleum geology. Acta Petrolei Sinica (in Chinese), 33(2): 188–194

Zhao Yingdong, Gan Huajun, Chen Shanbin, et al. 2015. Determination of Zhu-Qiong movement: The enlightenment from tectonic and sedimentary characteristics of Fushan Sag, Beibuwan Basin. Geology in China (in Chinese), 42(4): 948–959

Zheng Rongcai, Zheng Zhe, Gao Boyu, et al. 2013. Sedimentary features of the gravity flows in submarine fan of Zhujiang Formation in Baiyun Sag, Pearl River Mouth Basin. Lithologic Reservoirs (in Chinese), 25(2): 1–8

Zhu Yanhe, Zhu Weilin, Xu Qiang, et al. 2009. Sedimentary characteristics and sequence framework of the Zhuhai-Zhujiang Formation in the middle area of Pearl River Mouth Basin. Marine Geology & Quaternary Geology (in Chinese), 29(4): 77–83